JOURNAL OF GEOPHYSICAL RESEARCH, VOL. 113, D08304, doi:10.1029/2007JD009297, 2008

Direct measurement of biosphere-atmosphere isotopic CO_2 exchange using the eddy covariance technique

T. J. Griffis,[1] S. D. Sargent,[2] J. M. Baker,[3] X. Lee,[4] B. D. Tanner,[2] J. Greene,[2] E. Swiatek,[2] and K. Billmark[1]

Received 20 August 2007; revised 11 December 2007; accepted 14 January 2008; published 23 April 2008.

[1] Quantifying isotopic CO_2 exchange between the biosphere and atmosphere presents a significant measurement challenge, but has the potential to provide important constraints on local, regional, and global carbon cycling. Past approaches have indirectly estimated isotopic CO_2 exchange using relaxed eddy accumulation, the flask-based isoflux method, and flux-gradient techniques. Eddy covariance (EC) is an attractive method because it has the fewest theoretical assumptions and the potential to give a direct measure of isotopic CO_2 flux, but it requires a highly sensitive and relatively fast response instrument. To date, no such field measurements have been reported. Here we describe the use of a closed-path tunable diode laser absorption spectroscopy and eddy covariance (EC-TDL) system for isotopic ($C^{16}O_2$, $^{13}CO_2$, $C^{18}O^{16}O$) flux measurements. Results are presented from an intensive field experiment conducted over a soybean canopy from 18 July to 20 September 2006. This experiment represents a rigorous field test of the EC-TDL technique because the transport was dominated by relatively high frequency eddies. Net ecosystem CO_2 exchange (F_N) measured with the EC-TDL system showed strong correlation ($r^2 = 0.99$) in the half-hourly fluxes with an EC open-path infrared gas analyzer (EC-IRGA) over the 60-d period. Net CO_2 flux measured with the EC-IRGA and EC-TDL systems agreed to within 9%. Flux loss associated with diminished frequency response beyond 1 Hz for the EC-TDL system was approximately 8% during daytime windy (>4 m s^{-1}) conditions. There was no significant evidence of a kinetic-type fractionation effect related to a phase shift among isotopologues due to tube attenuation. Investigation of isotopic spectral similarity in the flux ratio (δ_N^x) for both $^{13}CO_2$ and $C^{18}O^{16}O$ transport showed that δ_N^x was relatively independent of eddy scale for this ecosystem type. Flux loss, therefore, did not significantly bias δ_N^x. There was excellent agreement between isofluxes (F_δ^x) measured using the flux-gradient and eddy covariance methods. Application of the EC-TDL technique over rougher surfaces or below canopy, where the flux-gradient approach is difficult to apply, appears promising for obtaining continuous long-term measurements of isotopic CO_2 exchange.

Citation: Griffis, T. J., S. D. Sargent, J. M. Baker, X. Lee, B. D. Tanner, J. Greene, E. Swiatek, and K. Billmark (2008), Direct measurement of biosphere-atmosphere isotopic CO_2 exchange using the eddy covariance technique, *J. Geophys. Res.*, *113*, D08304, doi:10.1029/2007JD009297.

1. Introduction

[2] In the late 1930s, physicist Alfred Nier pioneered one of the first isotope ratio mass spectrometers and conducted some of the first carbon isotope ratio measurements [*Murphey and Nier*, 1941; *Nier*, 1947]. Continued development of stable isotope theory and techniques over the last 70 years has provided important tools for studying a broad range of earth-system processes [*Hoefs*, 2004]. Quantifying isotopic CO_2 exchange between the biosphere and atmosphere has the potential to yield important insights into local, regional, and global carbon cycling [*Farquhar et al.*, 1989; *Keeling*, 1958; *Tans et al.*, 1993]. Application of stable isotope techniques to land-atmosphere CO_2 exchange problems has unfortunately been limited because of the inability to quantify the rapid fluctuations of isotopic CO_2 composition within boundary layer flows. Recently, new technologies including tunable diode laser (TDL) spectroscopy have been developed that will undoubtedly increase our capacity to acquire isotopic concentration and flux data with improved temporal and spatial resolution [*Bowling et al.*, 2003; *Griffis et al.*, 2004; *Lee et al.*, 2005].

[1]Department of Soil, Water, and Climate, University of Minnesota-Twin Cities, St. Paul, Minnesota, USA.
[2]Campbell Scientific, Inc., Logan, Utah, USA.
[3]USDA-ARS and Department of Soil, Water, and Climate, University of Minnesota-Twin Cities, St. Paul, Minnesota, USA.
[4]School of Forestry and Environmental Studies, Yale University, New Haven, Connecticut, USA.

0148-0227/08/2007JD009297$09.00

[3] Direct measurement of isotopic CO_2 exchange between the biosphere and atmosphere should provide some of the fundamental information needed to test the underlying theory for partitioning net ecosystem CO_2 exchange (F_N) into its gross components using stable isotope methods [*Bowling et al.*, 2001; *Yakir and Sternberg*, 2000; *Yakir and Wang*, 1996]. Further, isotopic fluxes can provide important diagnostic information that can be used to better understand changes in water use efficiency [*Ponton et al.*, 2006], help discern the dominant substrate types consumed during respiration [*Griffis et al.*, 2005a], and to interpret changes in atmospheric composition related to climate variations and land disturbance [*Welp et al.*, 2006]. It remains an important challenge and goal to complement efforts within the carbon cycle modeling community to help constrain inverse techniques [*Fung et al.*, 1997] by providing much needed data and parameters at improved spatial and temporal resolution. Further developments in laser spectroscopy and micrometeorological applications will help to address these important issues.

[4] Quantifying isotopic CO_2 transport between the biosphere and atmosphere represents a significant measurement challenge. The major limitation has been the lack of suitable fast-response analyzers capable of measuring isotopic ($C^{16}O_2$, $^{13}CO_2$, $C^{18}O^{16}O$) mixing ratios at the required precision for biosphere-atmosphere investigations. Past approaches have estimated isotopic CO_2 exchange using relaxed eddy accumulation (REA), the EC/flask isoflux method, and flux-gradient techniques [*Bowling et al.*, 1999, 2001; *Yakir and Wang*, 1996; *Griffis et al.*, 2004]. Each method has its advantages, disadvantages, and logistical challenges.

[5] REA has been used to measure both the carbon and oxygen isotope composition of CO_2 transport over forests [*Bowling et al.*, 1999]. The main challenge is to resolve isotopic differences in the separated updraft and downdraft air streams captured in flasks using mass spectrometry. While this approach has been used in the short term with some success, it is not suited to longer-term campaigns because of the large number of flasks and time required for analysis. REA requires a relatively large dead-band ($\pm 0.8\sigma_w$) to resolve the small differences in scalar mixing ratios between the updrafts and downdrafts. *Baker* [2000] demonstrated that the use of a dead-band generally reduces random noise in REA flux estimates. A dead-band, however, ultimately limits the sampling to only the largest eddies. This limits the amount of analyte and requires isotopic similarity with respect to eddy scale. A dead-band also directly impacts the value and physical interpretation of the REA proportionality coefficient, β. This parameter is derived from the statistical relationship between joint Gaussian distributions having a theoretical value of approximately 0.62 [*Baker*, 2000], but empirical studies have shown β to vary for different scalars and among sampling periods [*Baker*, 2000; *Katul et al.*, 1996].

[6] The EC/flask approach [*Bowling et al.*, 1999, 2001] relies on air captured in flasks over time periods ranging from a few minutes to a day to determine the relation between the isotope ratio (δ_a^{13}) and the CO_2 mixing ratio of air. This relation is then used to estimate high-frequency (i.e., 10 Hz) fluctuations in $^{13}CO_2$ on the basis of real-time high-frequency measurements of total CO_2 mixing ratio. The covariance of this $^{13}CO_2$ estimate with fluctuations in vertical wind velocity provides an approximation of the $^{13}CO_2$ flux. The fundamental limitation with the EC/flask approach is that it uses a very limited set of flask measurements to characterize the dynamic behavior of isotopic fluctuations in the atmosphere that occur over a broad range of temporal scales (seconds to hours). Other potential limitations to this approach include: uncertainty in the transfer function parameters given the limited range in CO_2 mixing ratio that is typically observed at shorter time intervals (i.e., minutes); the mismatch between the concentration (flask data) and the flux (EC data) footprints, which is problematic if terrain is heterogeneous [*Griffis et al.*, 2007]; and the assumption that there are only two end-members, which is an optimistic view when considering the $C^{18}O^{16}O$ flux [*Ogée et al.*, 2004].

[7] The flux-gradient method and Monin-Obukhov similarity theory have been applied to isotopic transport of CO_2 over agricultural surfaces [*Yakir and Wang*, 1996; *Griffis et al.*, 2004] and water vapor over forests [*Lee et al.*, 2007]. Recent studies have demonstrated that the TDL technique can greatly increase the temporal resolution of isotopic flux transport, yet it remains a very challenging task to resolve the relatively small daytime gradients above both agricultural and forest ecosystems. While the sampling methodology has improved considerably over the last few years to help resolve such small gradients, there are the usual concerns associated with gradient measurements including a potential mismatch in footprint for each inlet, counter-gradient transport, decoupling of the mixing ratio gradient from the local vertical flux density within the roughness sublayer, nonuniform sink/source distribution, etc. [*Kaimal and Finnigan*, 1994; *Raupach*, 1989].

[8] The limitations inherent in each of these techniques provides motivation to apply the eddy covariance (EC) approach [*Swinbank*, 1951] to the carbon isotope transport problem, which has a number of fundamental advantages:

[9] 1. It measures scalar transport between the biosphere and the atmosphere at relatively large spatial scales (ecosystem) and this measurement footprint is more consistent and better defined than for the flux-gradient or EC/flask approaches.

[10] 2. It provides continuous measurement at higher temporal resolution (hourly) than is practical with a flask-based approach.

[11] 3. Compared to other micrometeorological approaches, such as REA, flux-gradient or Monin-Obukhov similarity theory, it has the fewest underlying assumptions.

[12] 4. The EC approach can be used to study within-canopy turbulent exchange processes where gradient techniques break down because of concentration plumes originating from near-field sources [*Blanken et al.*, 1998].

[13] 5. Gradient measurements require that two inlets produce unbiased data for each isotopologue: four measurements are required to obtain the isotope flux ratio, which is a fairly stringent requirement over extended field campaigns. The EC application requires only a single inlet, thereby eliminating a potential source of bias.

[14] *Saleska et al.* [2006] have examined the feasibility and instrument requirements needed in order to quantify isotopic fluxes directly using the EC approach. At the present time, however, field measurements of the isotopic

fluxes via the EC method have not yet been reported. The purpose of this paper is to test the feasibility of making continuous EC measurements of isotopic CO_2 exchange ($^{13}CO_2$, $C^{16}O_2$, $C^{18}O^{16}O$) using tunable diode laser spectroscopy. A number of technical challenges were addressed: First, a sampling system and interpolation method were developed to calibrate raw isotopic mixing ratios point-by-point at 20 Hz; Second, instrument nonlinearity and temporal stability were evaluated; Third, the effects of high-frequency tube attenuation and its impact on flux loss and isotopic kinetic fractionation were examined; Finally, the impact of sample data gaps (30-s duration) resulting from instrument calibration at 5-min intervals was evaluated.

2. Theory and Methodology

2.1. Mass Conservation of Biosphere-Atmosphere Isotopic CO_2 Exchange

[15] A central goal of carbon cycle studies is to better understand the magnitude of gross ecosystem photosynthesis (F_{GEP}) and total ecosystem respiration (F_{TER}) and to determine how climate variations and land use change may alter these separate processes and impact the composition of the atmosphere. The net ecosystem CO_2 exchange (F_N) represents the small difference between these opposing processes

$$F_N = F_{GEP} + F_{TER}. \tag{1}$$

A positive sign indicates a flux leaving the surface (respiration) and a negative sign indicates a flux toward the surface (photosynthesis). F_N is now measured at about 400 sites globally using traditional open and closed-path infrared gas analyzer (IRGA) and EC systems (http://www-eosdis.ornl.gov/FLUXNET/). With the addition of stable carbon isotope information it should be possible to better constrain estimates of photosynthesis and respiration and to help interpret changes in atmospheric composition driven by changes in biospheric processes or anthropogenic activity.

[16] The isotopic mass balance for $^{13}CO_2$ or $C^{18}O^{16}O$ exchange (F_N^x) can be written as,

$$F_N^x = F_{GEP}^x + F_{TER}^x, \tag{2}$$

where, the superscript x indicates the $^{13}CO_2$ or $C^{18}O^{16}O$ isotope, and F_{GEP}^x and F_{TER}^x are the isotopic fluxes associated with gross ecosystem photosynthesis and total ecosystem respiration, respectively. In most field applications, however, isotopic partitioning is used to provide a constraint on canopy net photosynthesis ($F_A = F_{GEP} + F_L$) and nonfoliar ecosystem respiration ($F_R = F_{TER} - F_L$), where F_L is foliar respiration [*Lloyd et al.*, 1996; *Zobitz et al.*, 2007],

$$F_N = F_A + F_R \tag{3}$$

$$F_N^x = F_A^x + F_R^x. \tag{4}$$

To date, measurements of F_N^{13} and F_N^{18} have been rare because isotopic mixing ratios have been difficult to quantify reliably on a routine basis and at the required frequencies needed for atmospheric research [*Bowling et al.*, 1999, 2001; *Yakir*, 2003].

[17] The isotopic mass balance equation (4) has been approximated as [*Bowling et al.*, 2003]

$$R_N^x F_N = R_A^x F_A + R_R^x F_R, \tag{5}$$

where R^x is the absolute molar isotope ratio (i.e., for $^{13}CO_2$, $R^{13} = {}^{13}C/{}^{12}C \approx {}^{13}C/({}^{12}C+{}^{13}C)$) of each flux component including net ecosystem CO_2 exchange (R_N^x), net ecosystem photosynthesis (R_A^x) and nonfoliar ecosystem respiration (R_R^x). In practice, delta notation (δ^x) is used instead of R^x to describe the isotopic composition of the flux components by making use of a standard isotope scale,

$$\delta^x = 1000\left(\frac{R^x}{R_{VPDB}^x} - 1\right), ‰, \tag{6}$$

where R_{VPDB}^x is the standard molar ratio based on the Vienna Peedee Belemnite scale. The isotopic mass balance equation can also be written using isofluxes, defined as the product of the flux and its isotopic composition,

$$F_\delta^x = \delta_A^x F_A + \delta_R^x F_R = \left(\delta_a^x - \Delta^x\right)F_A + \delta_R^x F_R, \tag{7}$$

where $F_\delta^x = \delta_N^x F_N$ is the isoflux and δ_a^x, δ_A^x, and δ_R^x are the isotopic composition of the canopy air, net ecosystem photosynthetic flux, and the ecosystem respiratory flux, respectively, and Δ^x is the flux-weighted canopy photosynthetic discrimination against $^{13}CO_2$ or $C^{18}O^{16}O$. Here we report our results as isotopologue fluxes and as isofluxes. The isoflux is not a direct approximation to the isotopologue flux. An isoflux is a product of a flux and its isotopic composition and, therefore, has different units and opposite sign convention. Isoflux values are typically positive during daytime growing season conditions and act to enrich the atmosphere with respect to $^{13}CO_2$ or $C^{18}O^{16}O$. Negative isoflux values are typical at night or during nongrowing season conditions and cause relative depletion of atmospheric $^{13}CO_2$ or $C^{18}O^{16}O$. The sign of the isoflux is, therefore, opposite to F_N and F_N^x.

[18] If δ_A^x, and δ_R^x are not equal, the ecosystem is said to be in isotopic disequilibrium and equations (3) and (7) can be combined to provide constraints on either flux partitioning (i.e., F_A and F_R) [*Bowling et al.*, 2001] or inversely, to obtain estimates of canopy-scale discrimination associated with photosynthesis and respiration [*Griffis et al.*, 2005a].

2.2. Eddy Covariance Isotopic Flux Approach

[19] Eddy covariance is routinely used to quantify the transport of a number of scalars with a primary physical limitation being the need for a fast response analyzer for the scalar of interest [*Leuning and Judd*, 1996]. Following Reynolds decomposition and averaging, F_N can be determined from

$$F_N = \overline{\rho_a}\,\overline{w'c'} + S_c = \overline{\rho_a}\int C_{wc}(f)df + S_c, \tag{8}$$

where ρ_a is the molar density of dry air, w is the vertical wind velocity, c is the total CO_2 molar mixing ratio, the

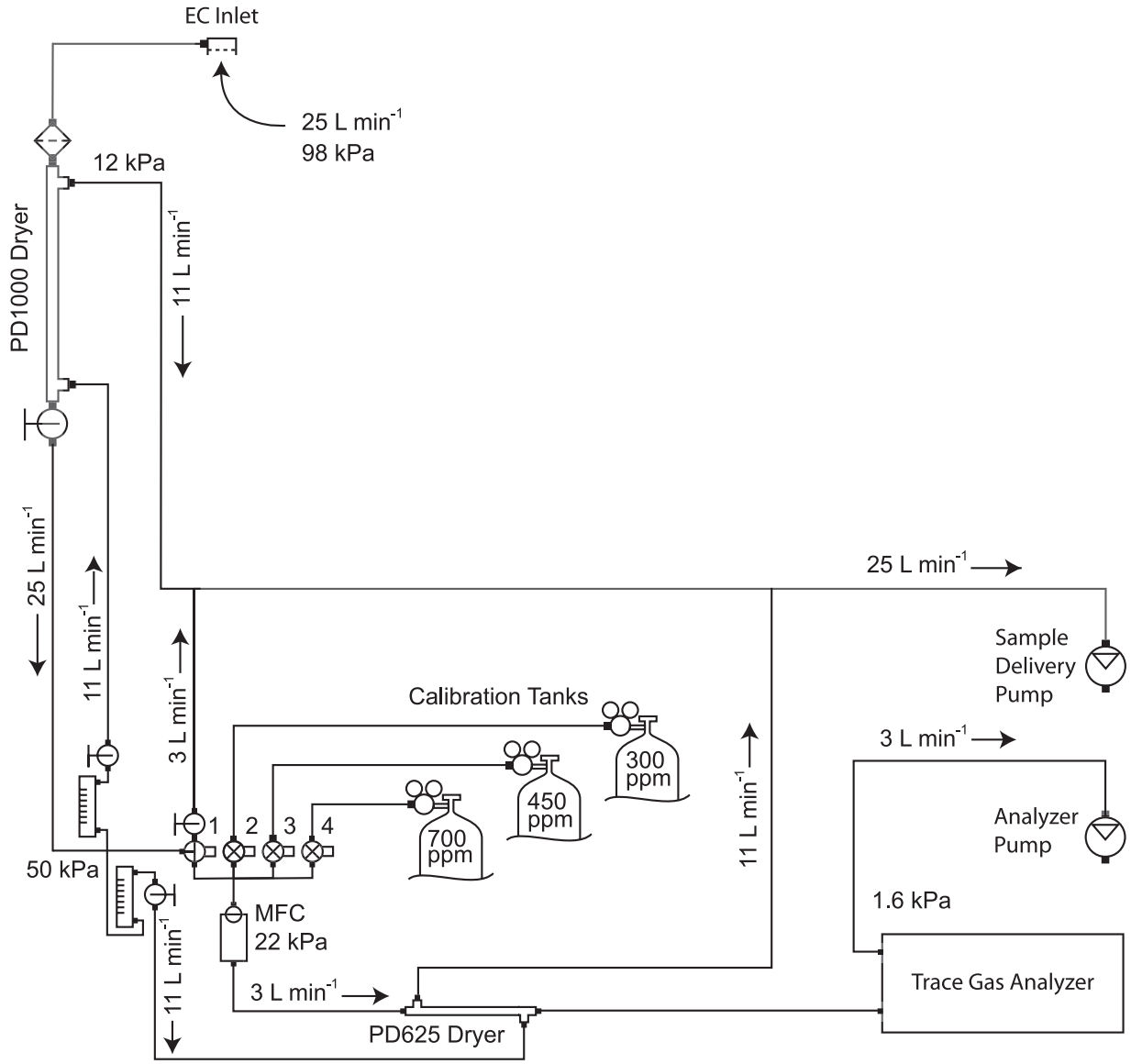

Figure 1. Diagram of the eddy covariance and tunable diode laser sampling system.

primes indicate the differences between instantaneous and mean values and the overbar indicates an averaging operation (30-min integration period is typical). Here $\overline{w'c'}$ is the mean covariance of w and c. Equivalently, F_N can be obtained from the cospectral density of the fluctuations in vertical wind velocity and CO_2 mixing ratio (C_{WC}), and f is the frequency of turbulent oscillations. S_c accounts for the rate of change in total CO_2 storage between the ground and the EC measurement height.

[20] The major measurement challenge has been determining the isotopic flux (left-hand side of equation (4)),

$$F_N^x = \overline{\rho_a}\overline{w'c^{x\prime}} + S_c^x = \overline{\rho_a}\int C_{wc^x}(f)df + S_c^x, \tag{9}$$

where, $\overline{w'c^{x\prime}}$ is the covariance of w and the heavy ($^{13}CO_2$ or $C^{18}O^{16}O$) molar mixing ratio, and S_c^x is the rate of change in $^{13}CO_2$ or $C^{18}O^{16}O$ storage between the ground and the EC measurement height. C_{wc}^x is the cospectral density of the fluctuations in vertical wind velocity and isotopic CO_2 mixing ratios.

[21] We often require the isotopic signature of flux components as a diagnostic of biospheric processes and function. In this case, EC flux ratios can be used to obtain the isotopic signatures of F_N from

$$R_N^x = \frac{\overline{w'c^{x\prime}}}{\overline{w'c^{12\prime}}}, \tag{10}$$

where the molar ratio (R_N^x) is computed from the ratio of the heavy to light isotope covariance terms and can be converted to delta notation using equation (6)

$$\delta_N^x = 1000\left(\frac{\overline{w'c^{x\prime}}/\overline{w'c^{12\prime}}}{R_{VPDB}^x} - 1\right). \tag{11}$$

If the flux ratio is computed in the absence of photosynthetic activity it represents the isotopic ratio of total

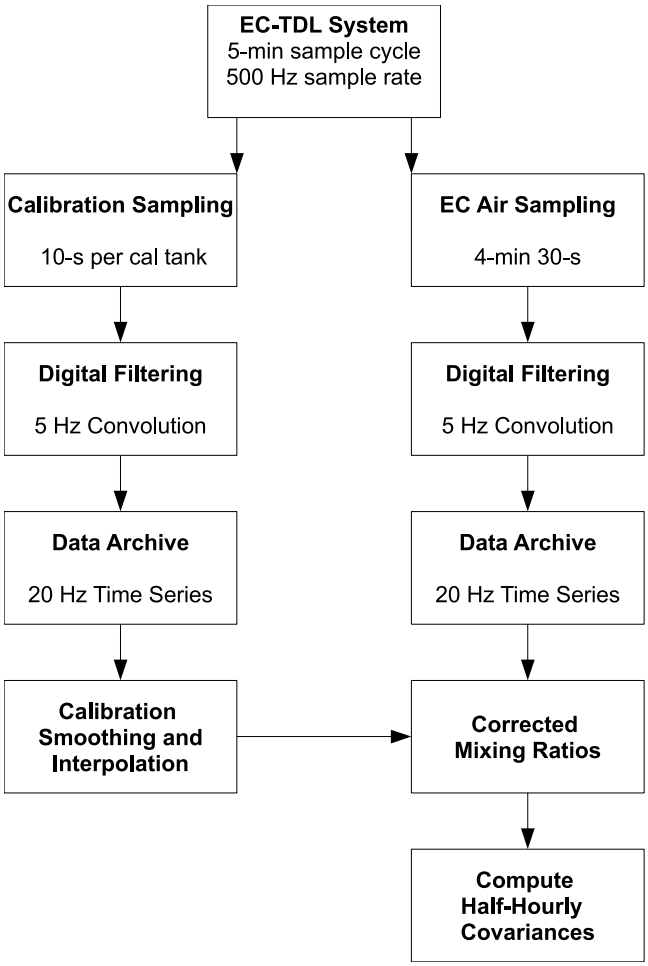

Figure 2. Data processing flow diagram describing data acquisition, filtering, calibration, and isotopic flux calculations.

ecosystem respiration, $\delta_R^x = \delta_N^x$. For historical reasons and ease of communication we express our results in delta notation and as isofluxes ($F_\delta^x = \delta_N^x F_N$), but note that the fundamental measurement is based on using equation (9). This requires that isotopic mole mixing ratios be calibrated against standard values based on the VPDB scale (i.e., reference material 8544, NBS19) as recommended by the International Union of Pure and Applied Chemistry, Commission on Atomic Weights and Isotopic Abundances [see *Griffis et al.*, 2004, Appendix A].

2.3. Tunable Diode Laser System

[22] In this study, $C^{16}O_2$, $^{13}CO_2$ and $C^{18}O^{16}O$ were measured in situ using the TDL (TGA100A, Campbell Scientific Inc., Logan, Utah, USA) method. The adaptation of this system for carbon isotope ratio studies was first described by *Bowling et al.* [2003]. Here we describe the upgraded analyzer and sampling system designed for the EC application. Each CO_2 isotopologue has unique absorption lines that can be selected and measured using midinfrared spectroscopy. Individual absorption line selection is accomplished by maintaining a low sample cell pressure (1.6 kPa), thereby reducing pressure broadening effects. In this experiment, $C^{16}O_2$, $^{13}CO_2$ and $C^{18}O^{16}O$ infrared absorption were measured at 2311.756, 2311.399, 2311.972 cm^{-1}, respectively with each measurement taking 2 ms (500 Hz total measurement rate). The 2 ms lag between the three isotopologues can cause significant errors in the isotope ratio if the concentrations vary rapidly in time. This problem is avoided by using digital filters with appropriate processing lags (746 ms for $C^{16}O_2$, 744 ms for $^{13}CO_2$, and 742 ms for $C^{18}O^{16}O$) to synchronize the measurements. For this study the 5 Hz EC filter passband option was selected to preserve the high frequencies, and the data were recorded at 20 Hz to avoid aliasing. This allowed the data to be digitally filtered in postprocessing to evaluate the trade-off between noise reduction and frequency response.

2.4. Air Sampling, Calibration Scheme, and Data Processing Methods

[23] The sample air stream was pulled at 25.0 L min^{-1} from the EC inlet located 0.1 m from the sonic anemometer path, through a 10-micron polypropylene filter and 47 mm filter holder (Pall Corporation 1235, NY, USA), a Nafion dryer (PD1000, Perma Pure Inc., NJ, USA) and Synflex tubing (Synflex Type 1300, 6.25 mm O.D. $\times$ 1.0 mm wall, Aurora, OH, USA) to a custom sampling system using a vacuum pump (RB0021, Busch Inc., Virginia Beach, VA, USA) (Figure 1). The sampling system selected either a subsample of the air stream from the EC inlet or one of three calibration cylinders. This subsample was pulled from the sampling system using a second Busch vacuum pump and was delivered to the TDL via a mass flow controller (16 M Series, Alicat Scientific, AZ, USA) at a rate of 3 L min^{-1}. A smaller Nafion dryer (PD625 Perma Pure Inc.) was positioned between the mass flow controller and the TDL to ensure air and calibration samples were at the same humidity. A 1.4 s time delay (28 samples at 20 Hz) between the sonic anemometer and TDL signals was caused by the 5 Hz digital filter (0.744 s) and the physical sample lag (0.66 s).

[24] The calibration scheme consisted of a three-point calibration using approximately 300, 450, and 700 μmol mol^{-1} CO_2 with known isotope ratios at 5-min intervals. Within each 5-min cycle each calibration inlet was sampled for 10 s and the subsampled air stream was sampled for 270 s. An omit time of 4 s (80 samples at 20 Hz) following valve switching was used to prevent bias related to residual sample air from the previous valve selection. All time series were recorded at 20 Hz. A linear or quadratic correction was obtained from the calibration measurements and used to determine the mixing ratios of the sample air.

[25] Net ecosystem CO_2 exchange was measured using two systems that shared the same sonic anemometer-thermometer (CSAT3, Campbell Scientific Inc.) including an open-path IRGA (LI-7500, Licor, NE, USA) and the closed-path EC-TDL system. The sonic anemometer-thermometer and open-path IRGA (EC-IRGA) were mounted at a height of 3.2 m (approximately 2.2 m above the zero plane displacement). Sensor separation was 0.1 m. As in all EC applications, it is not possible to sample the entire range of frequencies contributing to the flux. In this particular case, the limits on the integral terms in equations (8) and (9) are determined by the TDL system frequency response and the expected need to calibrate the TDL at 5-min intervals. If stationarity assumptions are satisfied [*Mahrt*,

Figure 3. Photograph of the eddy covariance and tunable diode laser (EC-TDL) system deployed at the University of Minnesota, Rosemount Research and Outreach Center, during the 2006 growing season. Isotopic flux measurements were made over a soybean canopy from 18 July to 20 September 2006.

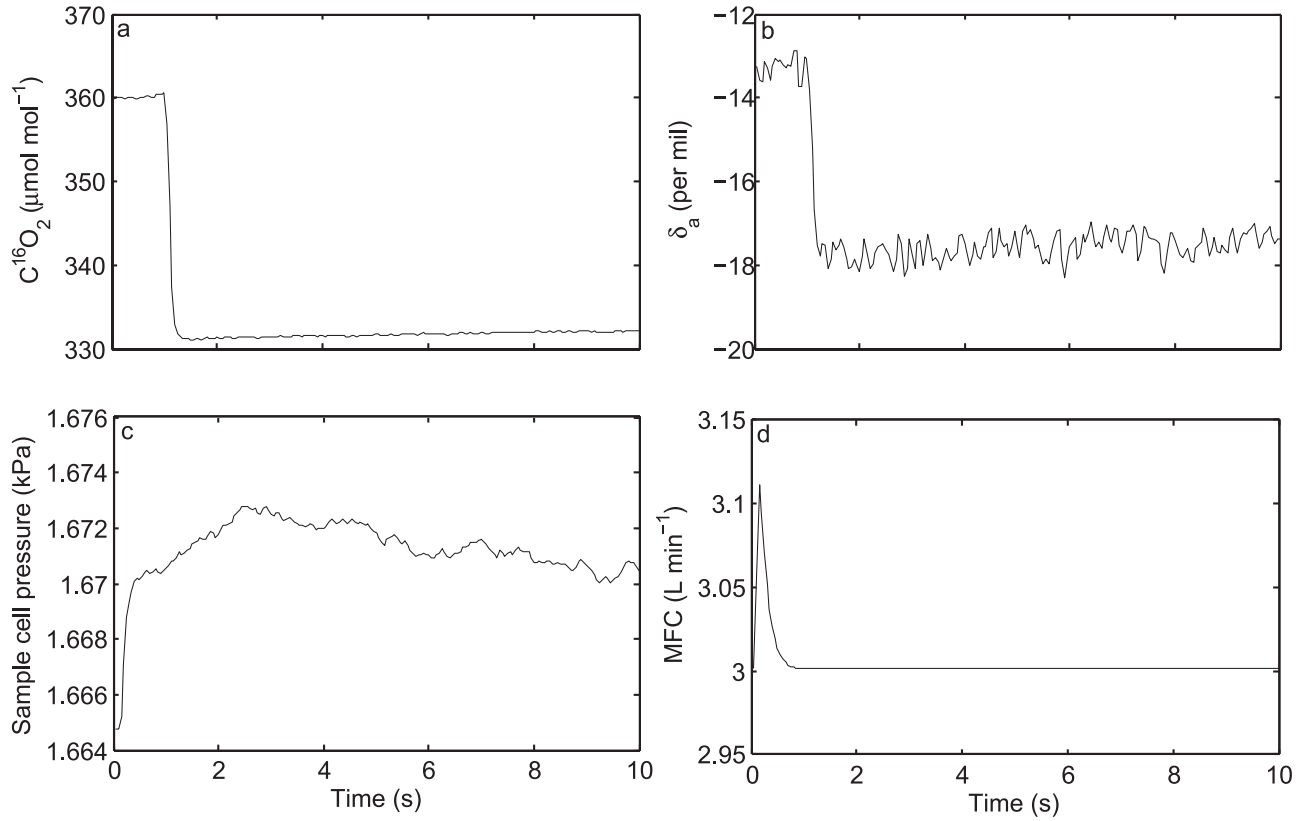

Figure 4. Transient response and equilibration time associated with valve switching: (a) uncalibrated $C^{16}O_2$ mixing ratio; (b) uncalibrated isotope ratio, δ_a^{13} ; (c) sample cell pressure; and (d) mass flow. Each plot is an ensemble average of all transitions from valve 1 (EC inlet) to valve 2 (calibration cylinder) over a 6-h period on 28 July 2006.

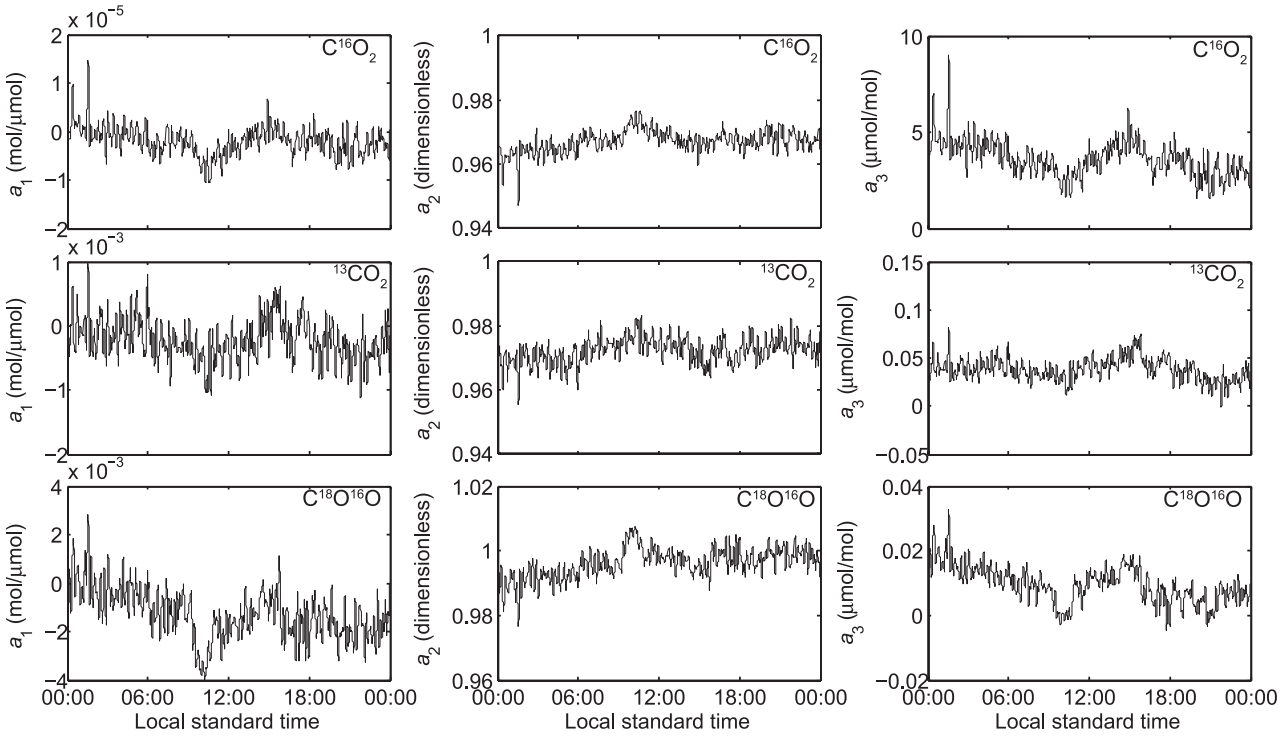

Figure 5. Quadratic calibration coefficients interpolated at 20 Hz for each isotopologue. The data shown are for 28 July 2006 (top) $C^{16}O_2$, (middle) $^{13}CO_2$, and (bottom) $C^{18}O^{16}O$ coefficients.

1998] each 4.5-min data block can be concatenated to quantify the flux at lower frequencies despite the gaps introduced during calibration. The effects of frequency response and calibration gaps on the isotopic flux data quality are described later.

[26] All postprocessing was performed using custom software developed in Matlab (The Mathworks Inc., Natick, MA, USA) and included the following.

[27] 1. A digital filter was applied to the raw mixing ratios. The filter was implemented using a Matlab convolution function using coefficients designed to give the same frequency response as the real-time filter options in the TDL software. This allowed us to explore the effects of digital filtering on flux and isotope ratio calculations. A 5 Hz filter was used for all subsequent analyses unless stated otherwise.

[28] 2. Calibration measurements at 5-min intervals were smoothed using a running mean function and these values were interpolated at 20 Hz between calibration intervals using a spline function.

[29] 3. First- and second-order calibration polynomials were computed from the interpolated calibration measurements for each isotopologue at 20 Hz. The air samples were corrected using each of these polynomials to explore the need for a nonlinear calibration (see Figure 2 for data processing sequence and calibration details).

[30] 4. The eddy flux for each isotopologue was obtained using traditional 30-min block averaging followed by coordinate rotation [*Baker and Griffis*, 2005]. In this case, the block averaging was based on all the non-omit data measured between the calibration intervals. There was no need to apply the traditional Webb, Pearman and Leuning (WPL) density terms [*Webb et al.*, 1980] because the sampled air was dried and temperature fluctuations were damped so that concentrations were expressed in terms of molar mixing ratios, not mole fractions. The WPL terms were applied to the EC-IRGA flux measurements.

2.5. Research Site and Supporting Measurements

[31] The experiment was conducted from 18 July to 20 September 2006 at the University of Minnesota, Rosemount Research and Outreach Center (RROC) located near St. Paul, Minnesota. This site is managed in a corn-soybean rotation. A detailed description of the site including aerial photographs, history of the site vegetation, and land use is given by *Griffis et al.* [2007]. The experiment described here was conducted during the soybean (*Glycine max*, C_3 photosynthetic pathway) phase of the rotation with planting taking place on 24 May 2006.

[32] The EC-TDL system was located approximately 50 m from the northern edge of the research field. The data are, therefore, sensitive to wind direction and must be filtered appropriately to exclude periods of northerly flow. Southerly flows produce an upwind fetch of about 350 m. The TDL system was operated in the field and was located 3 m from the tower. Figure 3 shows a photograph of the EC-TDL system during peak canopy growth.

[33] The site location was chosen because of access to AC power and to take advantage of an ongoing intensive carbon-water isotope exchange study involving two other TDL systems used for measuring water vapor and CO_2 isotopic gradients at an independent tower located within 15 m of the portable EC-TDL tower. These TDL systems

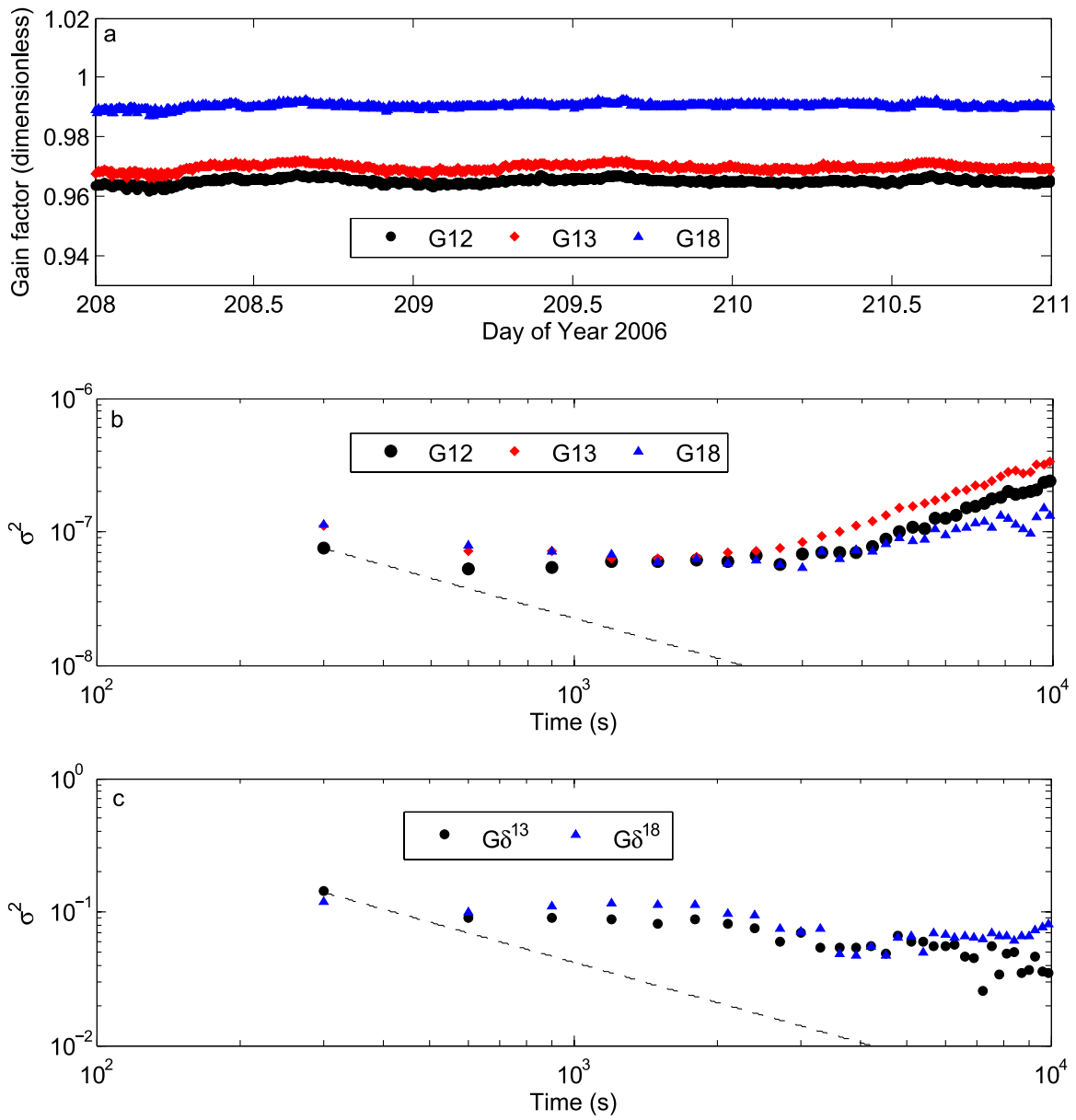

Figure 6. Allan variance analysis of the gain factors (linear calibration method) computed from each 5-min calibration interval over the period 26 to 29 July 2006. (a) Gain factors for $C^{16}O_2$, $^{13}CO_2$, and $C^{18}O^{16}O$. (b) Allan variance of the gain factors. (c) Allan variance of the isotope ratio gain factor, $G\delta^x = 1000\ (G^x/G^{12} - 1)$.

and the isotope gradient-diffusion and flux ratio techniques have been described previously by *Lee et al.* [2005] and *Griffis et al.* [2004]. The data from these measurement systems provide diagnostic information to help interpret the EC isotopic fluxes ($C^{16}O_2$, $^{13}CO_2$, $C^{18}O^{16}O$) and their flux isotope ratios [*Welp et al.*, 2008].

3. Results and Discussion

3.1. Phenology and Climate

[34] At the beginning of the experiment the leaf area index (LAI) was 6 $m^2\ m^{-2}$. A maximum LAI of 7.6 $m^2\ m^{-2}$ was attained by DOY 215 (2 August). LAI decreased rapidly after DOY 240 (27 August) and the canopy had fully senesced by DOY 254 (10 September). Over the same period canopy height increased from 0.6 to 1.2 m. The luxuriant canopy growth and large soybean yield (51 kg/ha) was the result of favorable temperatures and timely precipitation events. Mean air temperature over the course of the experiment was 20.3°C (30-year climate normal equals 21.0°C) with a minimum and maximum of 6.2°C and 36.0°C, respectively. Cumulative precipitation during the experimental period was 238 mm (30-year climate normal equals 116 mm).

3.2. EC-TDL System Performance

[35] The EC-TDL system was operated for 2315 half-hourly periods, equivalent to about 48 d, over the experi-

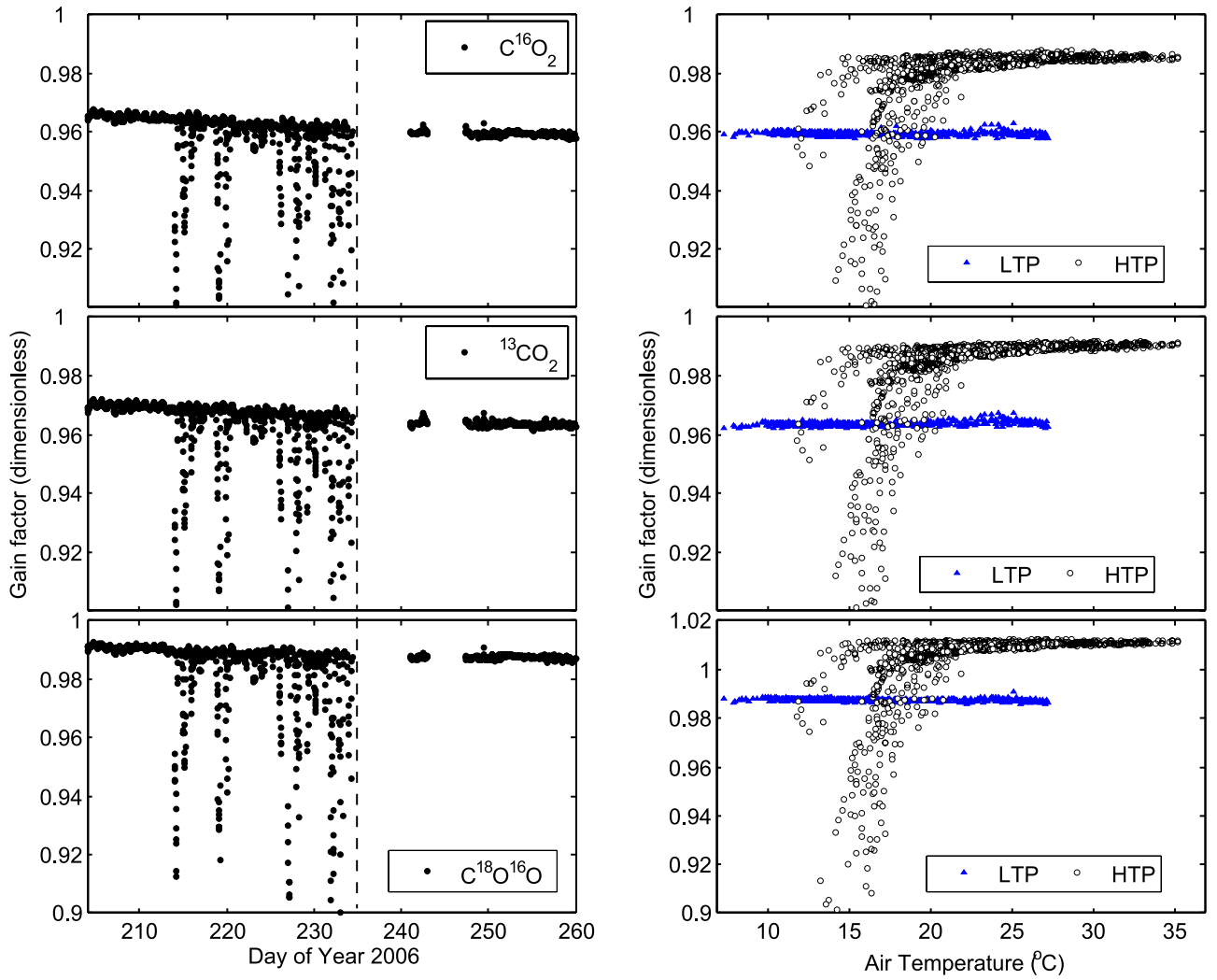

Figure 7. Long-term (55-d) variation in the calibration gain factors. (left) Gain factor for each isotopologue as a function of time. (right) Illustration of how the gain factor was influenced by air temperature and the reference gas cylinder pressure. Low tank pressure (LTP) and high tank pressure (HTP) are shown separately to demonstrate the impact of CO_2 condensation (i.e., high cylinder pressure at low temperatures) on the EC-TDL system performance. The vertical dashed line indicates the date when the reference cylinder pressure was reduced from 15 to 10 Mpa. Note that for clarity the HTP values have been increased by an offset factor of 0.02.

mental period. Some data gaps occurred because of regular maintenance that included refilling the laser dewar with liquid nitrogen (i.e., about 60-min data loss per 4 d), changing vacuum pump oil (about 30-min data loss per 30 d), and changing calibration cylinders (about 60-min data loss per 30 d). Three technical problems caused an additional data loss of 16.5%. The data logger occasionally fell behind in its processing instructions, causing it to switch the valves late. This problem was solved by updating the data logger operating system. CO_2 in the TDL reference gas cylinder (30% CO_2 balanced in air at 15 MPa) would condense when the ambient temperature fell below approximately 19°C. This problem was eliminated by reducing pressure in the reference cylinder to 10 MPa. Finally, the MFC flow performance degraded with time because of an O-ring being pulled into the flow path. The O-ring seal was changed to a design better suited to vacuum applications.

3.3. Calibration, Precision, and Stability

[36] Valve switching among the calibration and air sample inlets can cause uncertainty in the isotope ratio measurement because of pressure perturbations and residual sample air in the sample cell [*Griffis et al.*, 2005b]. We used a fast-response MFC and optimized its control coefficients to minimize flow and pressure perturbations. We omitted 4 s after each valve switch and applied a small step-change correction to minimize the effect of residual air in the sample cell. Figure 4 illustrates the transient response and equilibration of the system following a valve switch from the EC inlet (valve 1) to the first calibration inlet (valve 2, with calibrated values of CO_2 = 329.11 μmol mol^{-1} and δ^{13} = −11.9 ‰) repeated at 5-min intervals over a period of

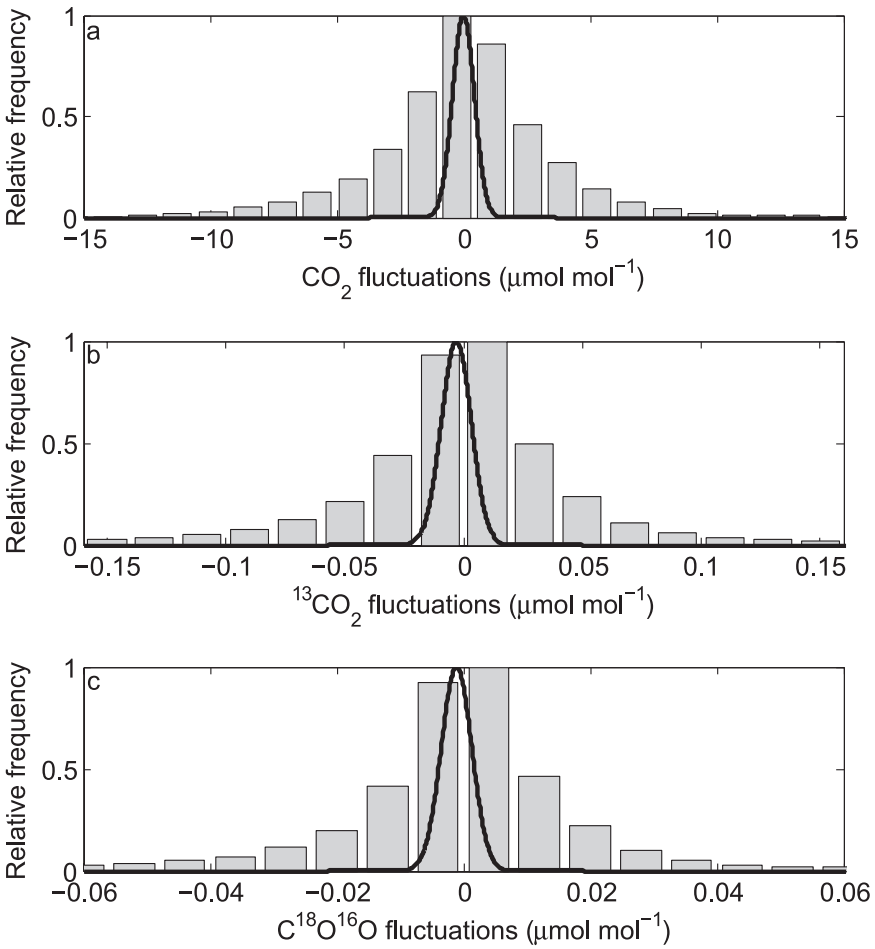

Figure 8. Histograms of the 20 Hz fluctuations of (a) CO_2 measured with the TDL, (b) $^{13}CO_2$ measured with the TDL, and (c) $C^{18}O^{16}O$ measured with the TDL. The data shown were measured over a 5-d period (26 to 30 July 2006). Note that the Gaussian curves represent the instrument noise.

6 h (1200 to 1800 local standard time) on 28 July 2006 (a "golden day" in terms of favorable meteorological conditions). The top panels show uncalibrated mixing ratio and carbon isotope ratio (ensemble average of all calibration intervals in the 6-h period). The $C^{16}O_2$ mixing ratio decreased rapidly starting 1.0 s after the valve switches, reaching within 1 μmol mol^{-1} of the final value 0.2 s later. There was a very small increase that continued to the end of the 10 s period. The isotopic ratio reached a stable value within about 0.2 s. The TDL pressure (lower left) showed little disturbance at the valve switch. The bottom right panel shows that the flow was perturbed 0.1 L min^{-1} and stabilized within 1 s. On the basis of these analyses, a conservative omit time of 4 s was used to minimize mixing ratio sample error following valve switching. A small step change correction (0.48% of the step change) reduced any bias in the measurement caused by not fully equilibrating at the new mixing ratio.

[37] Second-order calibration factors for $C^{16}O_2$, $C^{18}O^{16}O$ and $^{13}CO_2$, for 28 July 2006 are shown in Figure 5. The quadratic terms, in the left-hand panels, are nearly zero, indicating the nonlinearity of the TDL is very small. To evaluate the significance of the nonlinearity, we also calibrated these same data using a first-order polynomial, determined by linear regression on the three calibration standards. The corresponding means and standard deviations of the differences (i.e., quadratic – linear calibrated values), for $C^{16}O_2$, $C^{18}O^{16}O$, $^{13}CO_2$, δ^{13}, and δ^{18} were 0.0006 (±0.04) μmol mol^{-1}, 0.00005 (±0.0002) μmol mol^{-1}, 0.00008 (±0.0005) μmol mol^{-1}, 0.02 (±0.09)‰, and 0.03 (±0.08)‰, respectively. This comparison showed no significant difference between the two calibration techniques. The linear calibration approach has the advantage that it provides residuals to evaluate the quality of the fit. Therefore, we present all further results based on the linear calibration method.

[38] The covariance calculation removes any offset error in the measurements, so it is only the change in the linear calibration term (the gain factor) that affects the eddy flux and flux ratio calculation. A three-day time series of the gain factors for each isotopologue is shown in Figure 6a. The gain factors show very little variation, with no obvious diurnal pattern. The Allan variance [*Werle et al.*, 1993] of the gain factor (Figure 6b) shows that the calibration precision (square root of Allan variance, measured at 5-min intervals) was approximately 0.00027, 0.00034, and 0.00034 for $C^{16}O_2$, $^{13}CO_2$, and $C^{18}O^{16}O$, respectively. At 370 μmol mol^{-1}, this represents 0.1 μmol mol^{-1} for $C^{16}O_2$. The Allan variance is relatively flat, but it remains below this initial value until the averaging time is well beyond

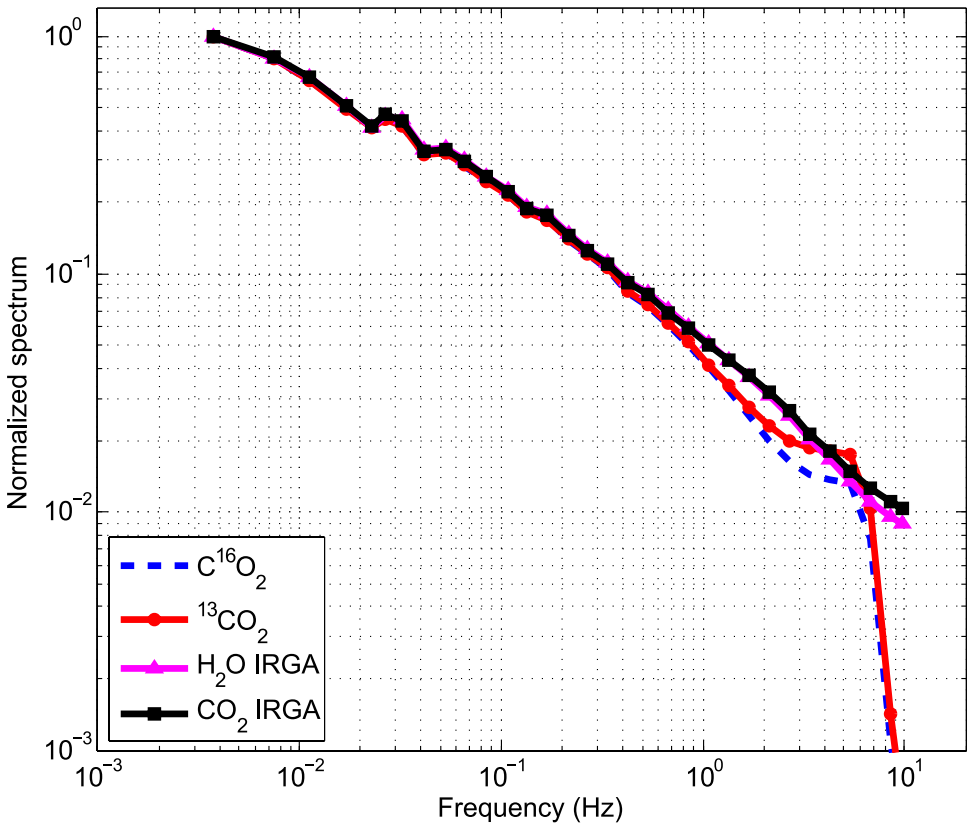

Figure 9. Spectral density analysis. Normalized spectrum of TDL and IRGA 20 Hz time series over a 3-h period (1200 to 1500 local time) on 28 July 2006 when winds were from the south and relatively constant at 4 m s^{-1}. Spectra were computed at 5-min intervals using Welch's averages periodogram method using Matlab. The spectra were bin-averaged using 10 logarithmically spaced intervals per decade.

1800 s (30 min). This suggests that the calibration precision could be improved slightly by averaging the calibrations over a period of 15 to 30 min, or alternatively, the calibrations could be performed less frequently with little loss of precision. Figure 6c shows the Allan variance analysis of the isotope ratio gain factor, ($G\delta^x$ = 1000 (G^x/G^{12}-1)), which indicates that the calibration precision of both isotope ratios was approximately 0.37‰ (square root of Allan variance, measured at 5-min intervals). Note that calibration precision of the isotope ratio gain factor was better than the propagated value (i.e., $\sqrt{0.27^2 + 0.34^2}$ = 0.43‰) from the individual gain factors because the errors tended to be correlated. This correlation keeps the isotope ratio Allan variance below its initial value even as the averaging time is extended to 10^4 s (nearly 3 h).

[39] The previous analyses showed the combined effects of instrument drift and noise on calibration measurements. To evaluate the precision of the TDL with the calibration process applied, we sampled from a cylinder of compressed air over a period of 22 h. The same 5-min calibration cycle was used as for the EC measurements. The mean mixing ratios were computed for each 4.5 min block, and isotope ratios were calculated using these values. The mean (±1 standard deviation) for the $C^{16}O_2$, δ^{13} and δ^{18} values were 345.31 (±0.04) μmol mol^{-1}, −9.41 (±0.26) ‰, and 3.59 (±0.24) ‰, respectively. The $C^{16}O_2$ precision was better than that reported by *Bowling et al.* [2003] and the δ^{13} precision was similar. Note that the δ^{13} precision could be improved by using stronger $C^{16}O_2$ and δ^{13} absorption lines [*Bowling et al.*, 2005], but these absorption lines do not allow for simultaneous measurement of $C^{18}O^{16}O$.

[40] The long-term (55-d) behavior of the gain factor for each isotopologue is shown in Figure 7. The large outliers during the midperiod of the measurement campaign were related to the reference gas CO_2 condensation events. After the reference tank pressure was reduced to 10 MPa the CO_2 condensation problem was eliminated and the stability of the system improved substantially.

[41] The standard deviation of the curve fit residuals, accounting for the degrees of freedom in the curve fits, was used to assess the long-term performance of the TDL. Using three calibration measurements to determine a calibration gain and offset leaves only one degree of freedom. Therefore this calculation is simply the square root of the sum of the squared residuals (RSSE). Median RSSE values for $C^{16}O_2$, $^{13}CO_2$, $C^{18}O^{16}O$, δ^{13} and δ^{18} were 0.12 μmol mol^{-1}, 0.0021 μmol mol^{-1}, 0.00054 μmol mol^{-1}, 0.18‰, and 0.19‰, respectively. Ninety-five percent of the RSSE values were below 0.27 μmol mol^{-1}, 0.0055 μmol mol^{-1}, 0.00013 μmol mol^{-1}, 0.60‰, and 0.55‰.

[42] The TDL short-term precision (noise) was evaluated under field conditions by measuring an air sample at 20 Hz (with 5 Hz passband filter) from a compressed air cylinder with known mixing ratio and isotope ratio over a 4.5-min interval. The uncalibrated mean (±1 standard

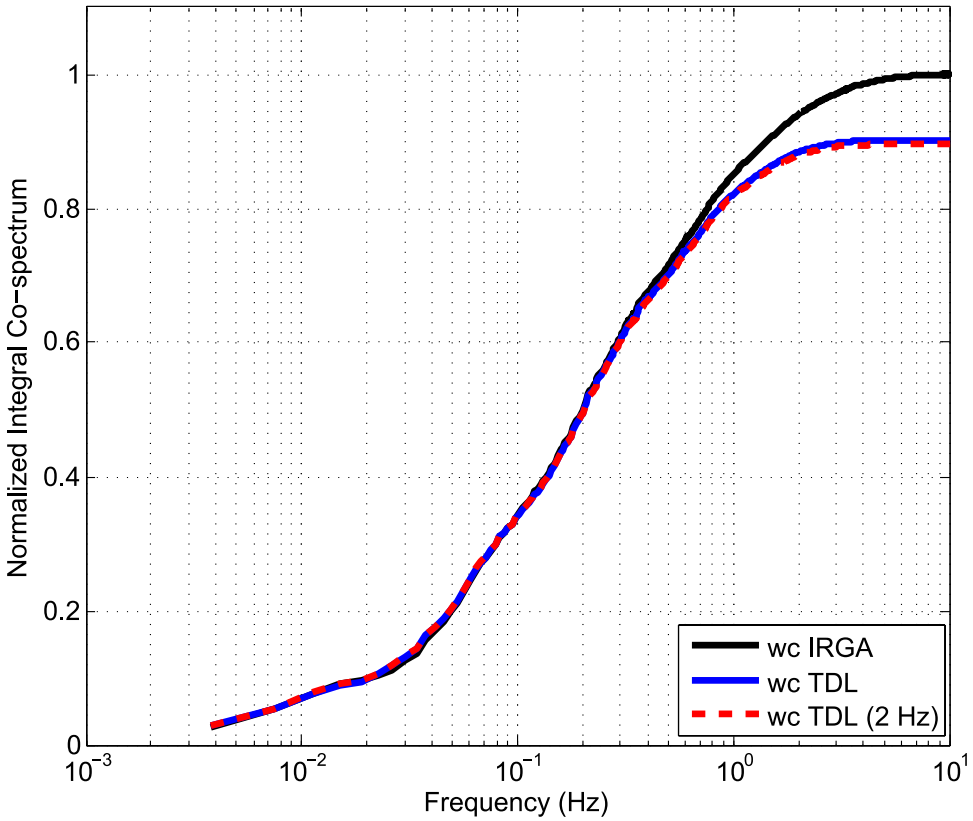

Figure 10. Cospectral density analysis. Normalized integral cospectral densities of vertical wind velocity (w) versus CO_2 mixing ratio measured with the TDL and IRGA. Cospectral densities were computed over a 3-h period (1200 to 1500 local time) on 28 July 2006 when winds were from the south and relatively constant at 4 m s^{-1}. Cospectra were computed at 5-min intervals using Welch's averages periodogram method using Matlab. Note that TDL (2Hz) indicates the application of a 2-Hz digital filter.

deviation) of $C^{16}O_2$, $^{13}CO_2$, $C^{18}O^{16}O$, δ^{13} and δ^{18} was 333.02 (±0.43) μmol mol^{-1}, 3.6643 (±0.0063) μmol mol^{-1}, 1.3439 (±0.0024) μmol mol^{-1}, −15.78 (±1.89) ‰, and −33.84 (±1.79) ‰, respectively. Measurement precision improved when using the 2 Hz passband filter. Values for $C^{16}O_2$, $^{13}CO_2$, $C^{18}O^{16}O$, δ^{13} and δ^{18} were 333.62 (±0.32) μmol mol^{-1}, 3.6709 (±0.0047) μmol mol^{-1}, 1.3463 (±0.0018) μmol mol^{-1}, −15.78 (±1.42) ‰, and −33.84 (±1.35) ‰, respectively. The TDL noise also depends on concentration. At higher CO_2 concentrations the mixing ratio noise increases and the isotope ratio noise decreases.

[43] To demonstrate the relation between instrument noise and ability to resolve actual fluctuations in CO_2 mixing ratios we compared the 20 Hz deviations, $c_a^{x\prime} = c_a^x - \overline{c_a^x}$, based on 5-min block averaging, to the short-term noise. Histograms of the fluctuations measured over a 5-d period (26 to 30 July 2006) are shown in Figure 8, with the instrument noise overplotted as a Gaussian curve. The CO_2 fluctuations measured with the TDL and IRGA had similar distributions with a standard deviation of 3.98 and 4.00 μmol mol^{-1}, respectively. The signal-to-noise ratio for the TDL CO_2 measurement was 12.4 compared to 25.0 for the IRGA. The standard deviations of the $c_a^{13\prime}$ and $c_a^{18\prime}$ values were 0.04 and 0.02 μmol mol^{-1} with corresponding signal-to-noise ratios of 8.5 and 11.1, respectively.

[44] *Saleska et al.* [2006] highlight the important fact that the EC approach does not require that all of the high-frequency fluctuations be resolved, but that the covariance between the vertical wind fluctuations and the scalar of interest be resolvable over the period of integration (i.e., 30 min). The contribution of instrument noise to flux uncertainty was estimated by computing the $C^{16}O_2$, $^{13}CO_2$, and $C^{18}O^{16}O$ fluxes with the EC sample air provided by a compressed air cylinder over a 12-h period (midnight to noon on 27 September 2006) under field conditions. These fluxes showed a near-normal distribution and the standard deviation was interpreted as the flux noise. The noise values were 0.21, 0.0020, and 0.00063 μmol m^{-2} s^{-1} for $C^{16}O_2$, $^{13}CO_2$, and $C^{18}O^{16}O$ fluxes, respectively. The relative flux noise, determined by comparing these noise values to typical flux values (i.e., median daytime values on 28 July 2006), was 1.4%, 1.3%, and 1.1%, respectively. After applying the 2 Hz digital filter the flux noise improved very slightly to 0.20, 0.0019, and 0.00061 μmol m^{-2} s^{-1}. We used the above approach and obtained isoflux (F_δ^{13}, F_δ^{18}) noise values of 168 (30%) and 138 μmol m^{-2} s^{-1} ‰ (67%), respectively. The 2 Hz digital filter had a very small impact on the flux noise compared to the more significant improvement in the instrument noise. This is a direct consequence of the spectral weighting of the vertical wind fluctuations. Since there is very little energy contained in the high-frequency vertical wind fluctuations the contribution of

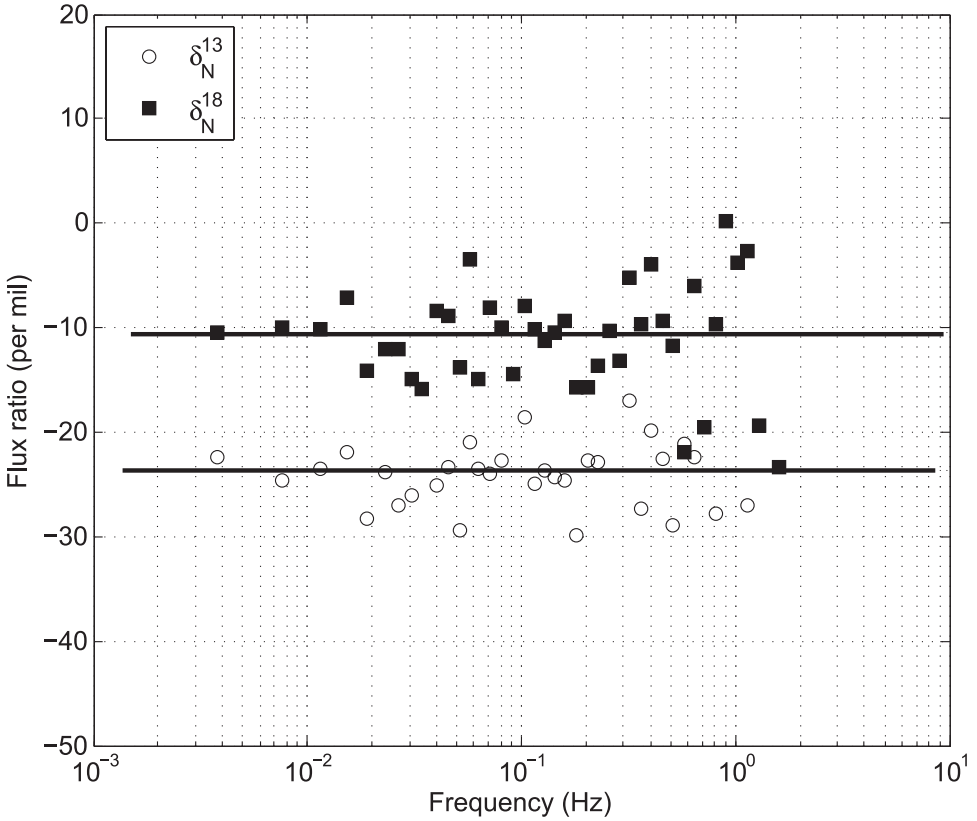

Figure 11. Investigation of isotope flux ratio spectral similarity. The isotopic composition of net ecosystem CO_2 exchange ($\delta_N{}^{13}$ and $\delta_N{}^{18}$) was computed from the ratio of cospectral densities and plotted in delta notation (‰) as a function of frequency. The cospectra were computed at 5-min intervals using Welch's averages periodogram method using Matlab. These analyses represent midday (1200 to 1500 local time) data collected from 23 to 29 July 2006. The dark solid lines indicate median values where $\delta_N{}^{13} = -23.7$ per mil and $\delta_N{}^{18} = -10.5$ per mil.

instrument noise at these same frequencies to the flux is negligible.

3.4. Sample Tube Attenuation and Kinetic Fractionation

[45] It is well known that in a closed-path system fluctuations in scalar concentrations are attenuated as the sample air is pulled through the tubing. The attenuation increases with increasing frequency, tube length, and at lower Reynolds numbers [*Lenschow and Raupach*, 1991; *Leuning and Judd*, 1996; *Massman*, 1991]. A potential deleterious effect on closed-path EC isotopic flux measurements is a kinetic-type fractionation resulting in a phase shift between the heavier and lighter isotope pairs. On the basis of molecular diffusivity, this effect would be most pronounced for $C^{18}O^{16}O/C^{16}O_2$ ratios, where the fractionation associated with laminar diffusion is 8.8‰. The ratio of the scalar concentration fluctuation at the point of sample tube entry versus a point downstream can be determined using the transfer function (equation (9) for laminar flow) of *Lenschow and Raupach* [1991]. For laminar flow through 9 m of tubing (a worst case scenario), the ratio decreased rapidly at frequencies >2.5 Hz. To evaluate potential differences among isotopic fluxes the tube transfer function for each isotope was applied to a common cospectrum of air temperature and vertical wind velocity ($C_{wT}(f)$) obtained at midday on 28 July 2006. The ratios of the integral cospectra for $^{13}CO_2/C^{16}O_2$ and $C^{18}O^{16}O/C^{16}O_2$ attenuation cases differed by 0.19‰ and 0.41‰, (integrated to 10 Hz) and indicate a small apparent fractionation introduced by tube attenuation under pure laminar flow. On the basis of observed and modeled variations in the isotopic composition of ecosystem respiration and photosynthetic discrimination the tube fractionation effect is likely to be insignificant under turbulent flow [*Zhang et al.*, 2006; *Knohl et al.*, 2005; *Baldocchi and Bowling*, 2003].

3.5. Spectral Analyses

[46] Spectra of the CO_2 mixing ratios measured with the TDL and IRGA are shown in Figure 9. These spectra were computed at 5-min intervals and averaged over a 3-h period (1200 to 1500 local standard time) for 28 July 2006 (DOY 209), when winds were relatively strong and constant (>4 m s^{-1}) from the south. This time period was selected to ensure a significant contribution of relatively high frequencies to the turbulent transport. The TDL ($C^{16}O_2$, $^{13}CO_2$) and IRGA (CO_2, H_2O) spectra show similar response at lower frequencies. The TDL response falls gradually farther below the IRGA starting at 0.5 Hz, as a result of tube attenuation and residence time (150 ms) of the sample cell volume (480 ml). The residence time is inversely related to the mass flow rate (3 L min^{-1}) and

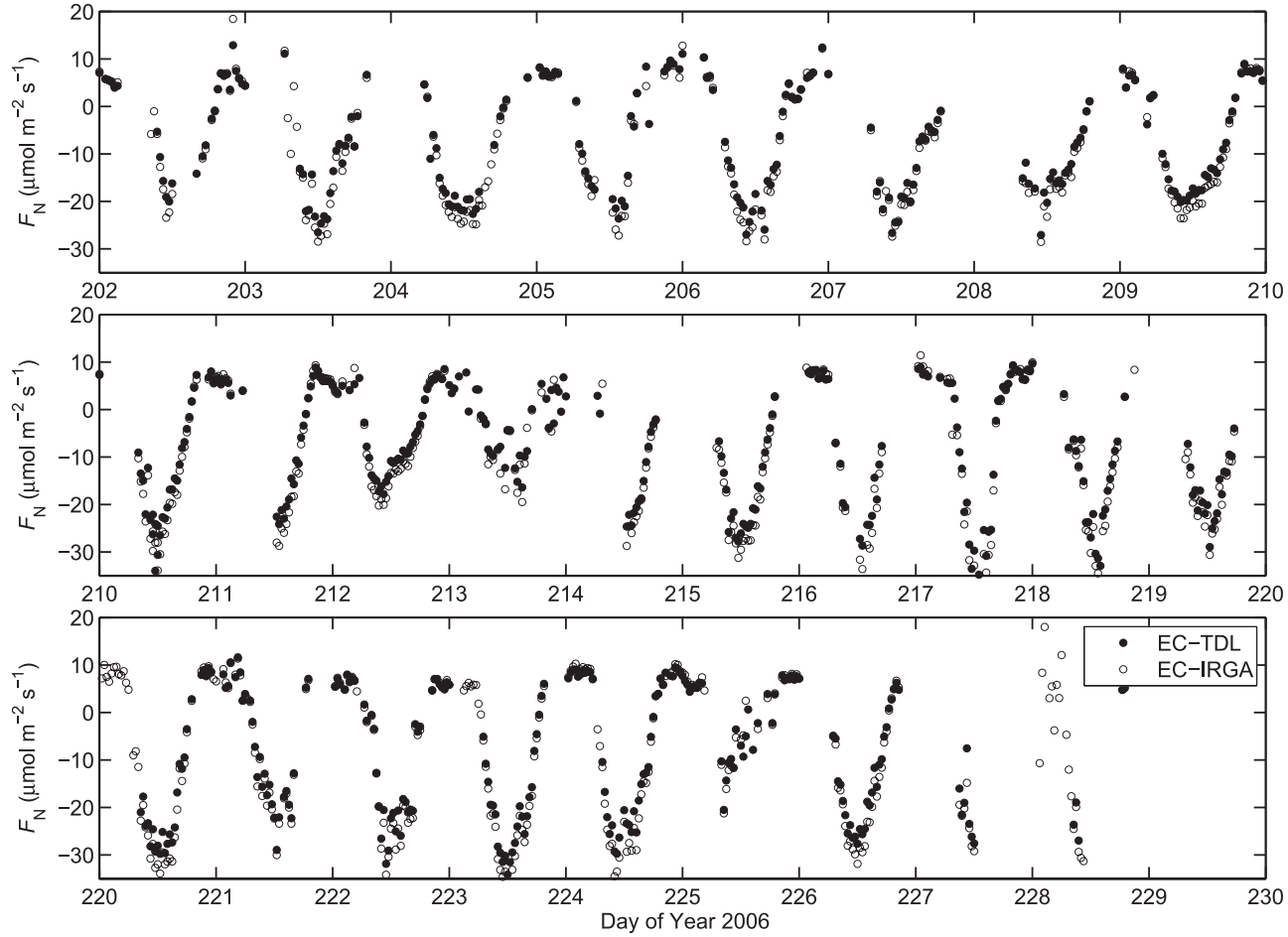

Figure 12. Time series of net ecosystem CO_2 exchange measured with the EC-IRGA and EC-TDL systems. Fluxes represent half-hourly values and were filtered according to low friction velocity ($u_* < 0.1$ m s^{-1}), high relative humidity (RH $\geq$ 98%), and precipitation and condensation events ($\lambda E < 0$ W m^{-2}).

directly related to the sample cell pressure (1.6 kPa). We note that the Reynolds number drops below the turbulent threshold (2300) through the nafion dryers and in the subsampled flow, which contribute to the frequency loss. While improved frequency response could be achieved at a higher subsampling flow rate, the unfortunate trade-off is reduced drying efficiency and increased consumption of calibration gases. The TDL spectra flatten out at the noise floor at 3 Hz and fall rapidly beyond 5 Hz, where the digital filter begins to attenuate the noise. The $C^{18}O^{16}O$ frequency response was nearly identical to $^{13}CO_2$ (for clarity these data are not shown in Figure 9).

[47] To what extent the lower relative frequency response of the TDL system influences the CO_2 flux measurement is dependent on the characteristics of the cospectrum of vertical wind and CO_2 fluctuations (C_{wc}). Over a relatively smooth surface such as soybean, and with a low sampling height, smaller eddies will account for a greater relative proportion of the scalar transport compared to rougher surfaces such as forests. The integral cospectrum, normalized by the total power, is shown in Figure 10 for the same time period (28 July 2006; DOY 209). This experiment, therefore, is a rigorous test of the EC-TDL system and illustrates that about 85% of the daytime scalar transport is contributed by eddy frequencies below 1 Hz. The integral cospectrum also indicates that during daytime windy conditions the EC-TDL system "misses" about 8% of the flux because of signal loss at the higher frequencies. This value may be exaggerated because the EC-IRGA system includes WPL corrections, which might be underestimated when there is a lack of energy balance closure [*Liu et al.*, 2006]. The turbulent fluxes of sensible and latent heat typically account for about 80% of the available energy at this research site [*Baker and Griffis*, 2005]. If the lack of energy balance closure is associated with underestimating the sensible and latent heat flux terms this would result in a smaller WPL term and, therefore, larger apparent CO_2 fluxes. The TDL integral cospectrum with the 2 Hz filter applied, also shown in Figure 10, confirms there is little additional flux loss associated with the lower filter passband. However, the flux noise estimated from the compressed air data showed little improvement with additional filtering. The nighttime normalized integral cospectra (data not shown) agreed to within 3%. This was a somewhat surprising result because scalar transport is dominated by higher frequencies during stable/nighttime conditions [*Kaimal and Finnigan*, 1994, Figure 2.18].

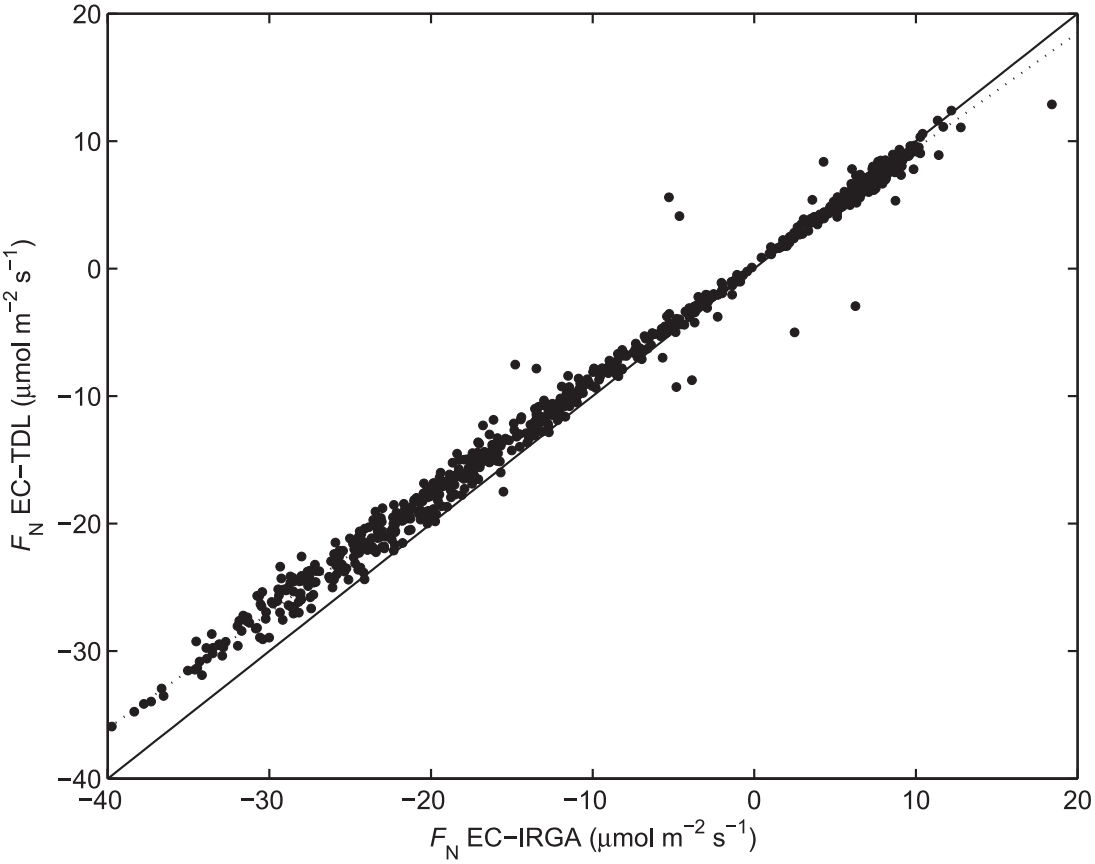

Figure 13. Comparison of net ecosystem CO_2 exchange measured with the EC-IRGA and EC-TDL systems. The solid line represents the 1:1 relation and the dashed line is a geometric regression fit with $y = 0.91x + 0.3$, $r^2 = 0.99$. Data shown are from Figure 12.

[48] Daytime and nighttime flux loss (i.e., the EC-TDL CO_2 flux divided by the EC-IRGA CO_2 flux) was examined as a function of mean horizontal wind velocity (u) for the period DOY 200 to DOY 230. Daytime flux loss (i.e., unstable atmospheric conditions) increased with increasing wind velocity ($y = -0.022u + 0.95$, $r^2 = 0.78$, RMSE = 0.04). This is a direct result of higher-frequency fluctuations under windy conditions and their attenuation [*Kaimal et al.*, 1972; *Lee et al.*, 1994]. Similar results were presented by *Lee et al.* [1994] who compared open- and closed-path EC-IRGA systems for measuring CO_2 exchange over a clover canopy. Their results indicated a flux loss of about 20% for wind velocities greater than 4.5 m s^{-1}. They also noted that the flux loss was significantly less than that predicted from the theory of tube attenuation of scalar fluctuations [*Leuning and Moncrieff*, 1990]. Our analysis also showed that given the same wind velocity at night (i.e., during stable conditions) there was less total flux loss, which was unexpected, yet consistent with the cospectral analyses above. The rate of flux loss, however, was greater at night ($y = -0.032u + 1.03$, $r^2 = 0.37$, RMSE = 0.06) compared to daytime, because eddies shift toward higher frequencies under stable conditions. We hypothesize that greater daytime flux loss was related to the fact that WPL terms must be applied to the EC-IRGA data. Therefore, lack of energy balance closure, as discussed above, could result in larger apparent CO_2 fluxes as measured with the EC-IRGA system. The effect would be most pronounced during daytime when sensible and latent heat fluxes are relatively large.

[49] The impact of calibration gaps at 5-min intervals on the half-hourly flux estimate was evaluated by simulating 30-s calibration gaps injected every 5-min into the raw 20 Hz EC-IRGA signal for 28 July 2006. Fluxes were then recomputed as described above using 30-min block averaging. On the basis of regression analyses the effect appeared to be insignificant, resulting in a flux loss of approximately 0.6% on average ($y = 0.994x + 0.036$, $r^2 = 0.99$, $n = 48$, RMSE = 0.32, where x is the CO_2 flux based on a continuous 20 Hz half-hourly block). It would appear therefore that frequent calibration has little impact on resolving the half-hourly covariance estimate.

[50] Flux loss related to attenuated frequency response of the EC-TDL system could impact the isotopic signature of F_N if eddy scale has an important influence on the isotopic composition of the CO_2 transported between the surface and atmosphere. For instance, larger eddies may penetrate the canopy and bear an isotopic signal more characteristic of the soil flux. *Bowling et al.* [2001] sampled air into flasks at various timescales and used carbon isotope ratio mass spectrometry analyses to examine these potential effects over a deciduous forest and did not find significant differences. It is likely that such an effect would be of greater importance for $C^{18}O^{16}O$ because differences between leaf and soil signatures may be on the order of about 20‰ [*Riley et al.,* 2003]. Flux loss related to frequency attenuation

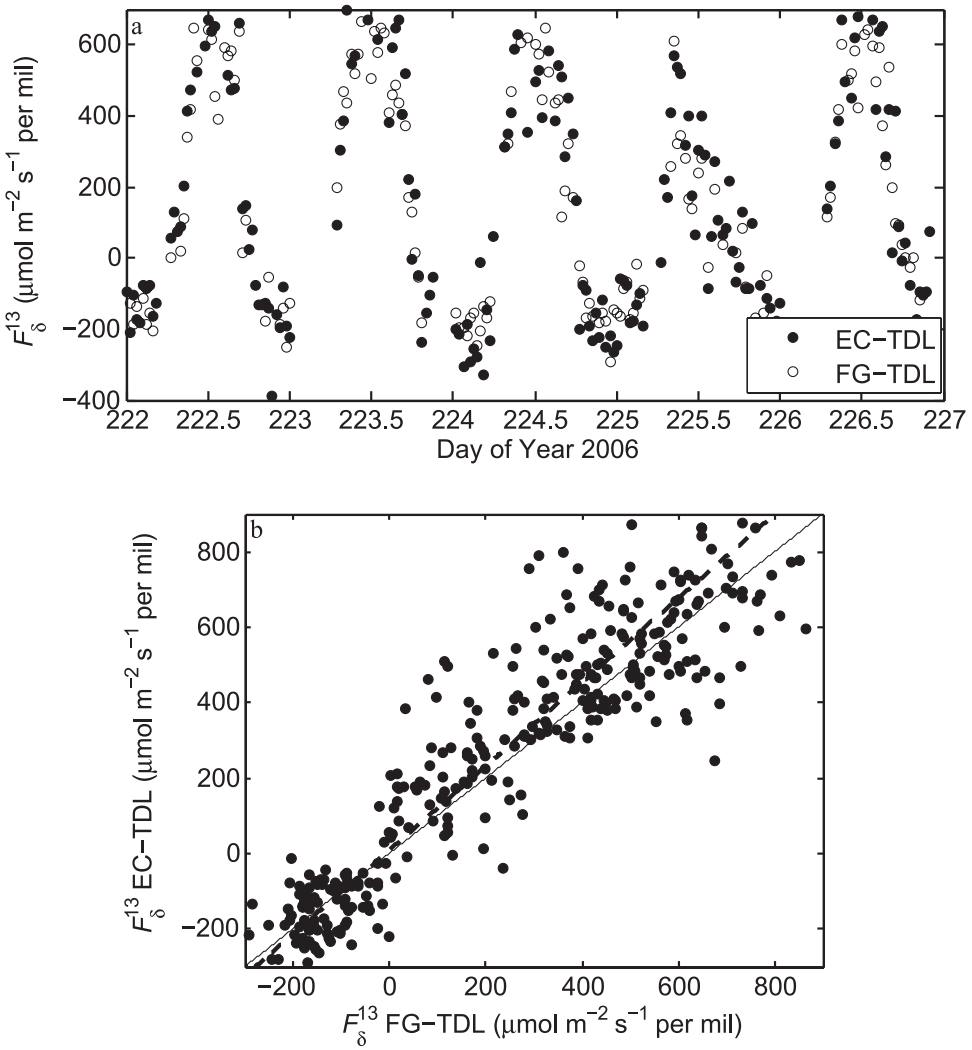

Figure 14. Patterns of isotopic CO_2 exchange. (a) Time series of flux-gradient and eddy covariance $^{13}CO_2$ isoflux. (b) Relationship between flux-gradient and eddy covariance $^{13}CO_2$ isoflux. The solid line represents the 1:1 relation, and the dashed line is a geometric regression fit.

could bias the isotope flux ratio of F_N if there is not isotopic spectral similarity. The data presented in Figure 11 show substantial variations in the isotope flux ratios as a function of eddy frequency, $\delta_N^x(f) = 1000\left(\frac{C_{wcx}(f)/C_{wc}(f)}{R_{VPDB}^x} - 1\right)$, but no significant trends were detected on the basis of regression analyses. Flux ratios beyond 2 Hz (where the flux is very small) become very noisy and are not shown in Figure 11. The EC-TDL flux underestimate over this soybean canopy should, therefore, not have a significant impact on quantifying the isotopic signature of the net CO_2 flux. This transport problem, however, deserves further attention over rougher surfaces where greater differences may be associated with large versus small eddy scales and can now be more thoroughly investigated given this improved capacity to resolve rapid fluctuations in $^{13}CO_2$ and $C^{18}O^{16}O$.

3.6. Net Ecosystem CO_2 Exchange, Isofluxes, and Flux Ratios

[51] Half-hourly F_N are shown in Figure 12 for the period DOY 202 to DOY 228. For this time series fluxes were filtered according to low friction velocity ($u_* < 0.1$ m s^{-1}) high relative humidity (RH $\geq$ 98%) and precipitation and condensation events ($\lambda E < 0$ W m^{-2}). The fluxes ranged from −35 to 20 μmol m^{-2} s^{-1}. Figure 13 shows the 1:1 plot of these same data. The high correlation between these systems over this range of environmental conditions is exceptional ($y = 0.91x + 0.30$, $r^2 = 0.99$, geometric regression). The combination of calibration blanking and the lower frequency response of the TDL system reduced the total CO_2 flux by about 9%, which is in excellent agreement with the cospectral analyses when both nighttime and daytime conditions are considered. The relatively good agreement between both systems indicates that there is no need to measure the total flux independently for isotopic flux partitioning [*Zhang et al.*, 2006], which has been a considerable limitation in previous approaches. Further, it should be possible to correct the flux loss on the basis of a cospectrum transfer function using sensible heat flux derived from the sonic temperature [*Massman*, 2000] by assuming spectral similarity.

[52] An example of the $^{13}CO_2$ isoflux time series, measured with the EC-TDL system and with a TDL flux-

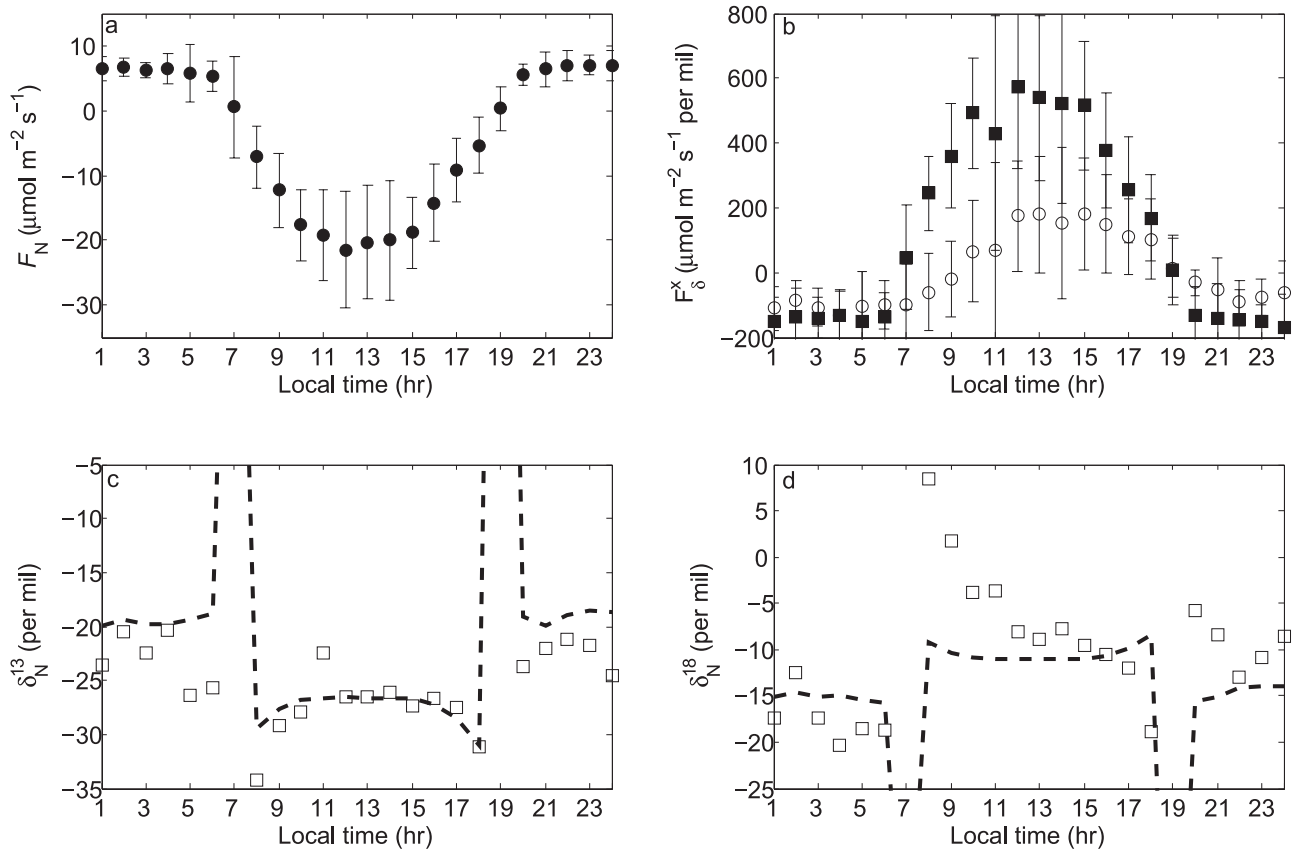

Figure 15. Diurnal ensemble average of (a) net ecosystem CO_2 exchange, (b) $^{13}CO_2$ (closed squares) and $C^{18}O^{16}O$ (open circles) isofluxes, (c) $\delta_N{}^{13}$, and (d) $\delta_N{}^{18}$ for the entire experimental period. Note that the flux ratios, $\delta_N{}^{13}$ and $\delta_N{}^{18}$, were derived by dividing the data in Figure 15b by Figure 15a. The dashed black lines in Figures 15c and 15d show simple simulations of $\delta_N{}^{13}$ and $\delta_N{}^{18}$ assuming an isotopic disequilibrium of −5 and +3 per mil, respectively with F_R = 6.5 μmol m^{-2} s^{-1} and $F_P = F_N - F_R$.

gradient system, is shown in Figure 14a and a comparative plot of all simultaneous data collected during the experiment is shown in Figure 14b. These data demonstrate relatively good agreement between both the EC and flux-gradient method, which should be expected over a short canopy when the gradient is resolved above the roughness sublayer [*Griffis et al.*, 2007; *Simpson et al.*, 1998]. On the basis of a two sample *t*-test (n = 258, 1% significance level), there was not a statistically significant difference between each of the approaches.

[53] Figure 15 shows the ensemble average diurnal variation in F_N, F_δ^x, and δ_N^x for all of the valid data measured over the experimental period. Note that the flux ratios, δ_N^{13} and δ_N^{18}, were derived by dividing the data in Figure 15b by Figure 15a. In the case of δ_N^{13}, the isotopic disequilibrium (difference between daytime and nighttime values) resulted from the differences in isotopic composition between F_R and F_A. Greater daytime $^{13}CO_2$ depletion can be attributed to the strong photosynthetic discrimination of the C_3 soybean canopy while F_R tended to be more enriched because the soil organic matter contains significant amounts of C_4 residue from many years of corn production. In the case of δ_N^{18}, isotopic disequilibrium is very complex, driven by simultaneous changes in the leaf and soil water isotopic composition and the equilibration of CO_2 with liquid water via the hydration reaction [*Hesterburg and Siegenthaler*, 1991; *Gillon and Yakir*, 2001; *Lee et al.*, 2007]. The data shown in Figure 15d show a similar diurnal pattern to that reported previously by *Griffis et al.* [2005b] for a soybean canopy. The positive δ_N^{18} values during midday appear to be caused by a change in the sign of the leaf retroflux (back diffusion of leaf CO_2 to the atmosphere). Isotopic water vapor and leaf water measurements during this period support that the daytime positive values of δ_N^{18} occurred when the daytime leaf water had an isotope signature that was positive in sign because of highly ^{18}O enriched leaf water [*Welp et al.*, 2008].

[54] The variability in δ_N^x increased substantially at low flux values, but was relatively well-behaved when $|F_N|$ exceeded 4 μmol m^{-2} s^{-1}. *Miller and Tans* [2003] noted emphatically that if the one-way fluxes differ in sign, then δ_N^x may not fall within the range of the isotope ratios of the individual fluxes (end-members). We simulated the δ_N^{13} and δ_N^{18} that would result from a constant F_R (6.5 μmol m^{-2} s^{-1}) with $F_A = F_N - F_R$ for a −5‰ and +3‰ disequilibrium, respectively. The resulting isotope ratios, shown in the lower panels of Figure 15 (black dashed lines), show a very similar pattern to the observed δ_N^{13}, but correlate poorly with δ_N^{18}. It is very important to note that small changes in the isotope ratio of F_A or F_R cause large changes in δ_N^x at low

F_N (near sunset and sunrise or 0700 and 1900 local time). These plots demonstrate that the "modeled" and measured δ_N^x variability is often simply related to variability in F_N at small flux values. This further highlights the need to interpret δ_N^x with caution.

4. Conclusions

[55] Eddy covariance and tunable diode laser spectroscopy were combined for the first time to directly measure isotopic fluxes of $C^{16}O_2$, $^{13}CO_2$, and $C^{18}O^{16}O$ above a soybean canopy over a period of 60 d and were compared to flux-gradient measurements. Development of this technique has been pursued for a number of fundamental reasons: This is likely the only suitable methodology capable of resolving isotopic fluxes over rough surfaces such as forests or from tall tower or aircraft platforms where gradients are extremely small and countergradient transport is significant; The flux ratio signal from the eddy covariance approach is likely more reliable when used within the roughness sublayer compared to gradient techniques; This approach provides an exciting opportunity to measure below-canopy isotopic fluxes to determine differences between soil and vegetation signals and to help resolve CO_2 recycling within the canopy; The new methodology should allow investigators to characterize how eddy scale (spatial and temporal) influences isotopic signatures of biosphere-atmosphere CO_2 transport.

[56] While this is a major advance in the application of micrometeorological and stable carbon isotope techniques there are practical limitations, especially for long-term operation at remote field sites, including: the need to refill the liquid nitrogen dewar every 5 or 6 d; the consumption of expensive calibration gases; and the significant power required for the sampling pumps. The system described here is best suited to locations with AC mains power available and with convenient access for transporting liquid nitrogen and calibration cylinders.

[57] On the basis of this feasibility test we conclude the following.

[58] 1. Net CO_2 flux measured with the eddy covariance and open-path infrared gas analyzer (EC-IRGA) and eddy covariance and tunable diode laser (EC-TDL) systems agreed to within 9%. Lower flux estimates measured by the EC-TDL system were related to high-frequency attenuation at frequencies beyond about 1 Hz.

[59] 2. There was no significant phase shift among isotopologues or kinetic isotope fractionation introduced by tube attenuation.

[60] 3. Spectral similarity in the flux ratios (δ_N^x) suggests that flux loss from high-frequency attenuation will have little impact on determining the isotopic signature of the net CO_2 flux over a relatively short canopy. The relation between eddy scale and isotopic transport requires further investigation especially for ecosystems of taller stature where there may be significant differences in the sink/source isotopic signals.

[61] 4. Typical daytime relative uncertainties for the isotopologue fluxes (F_N^{12}, F_N^{13}, F_N^{18}) and isofluxes ($F\delta^{13}$, F_δ^{18}) were 1.4%, 1.3%, 1.1%, 30%, and 67%, respectively.

[62] 5. There was excellent agreement in the isoflux values estimated using the EC and flux-gradient approaches, with similar precision. Application of the EC-TDL technique over rougher surfaces such as forests or within canopy, where flux-gradient methods are difficult to apply, shows considerable promise for long-term continuous isotopic measurements of both $^{13}CO_2$ and $C^{18}O^{16}O$.

Notation

Note that the superscript ^{x} indicates the isotopologue, $^{13}CO_2$ or $C^{18}O^{16}O$

a_1	quadratic calibration coefficient (nonlinear term), mol μmol^{-1}.
a_2	quadratic calibration coefficient (linear term), dimensionless.
a_3	quadratic calibration coefficient (offset), μmol mol^{-1}.
β	proportionality coefficient used in the relaxed eddy accumulation technique, dimensionless.
c	total carbon dioxide mole mixing ratio including all isotopologues, μmol mol^{-1}.
$c^{x\prime}$	20-Hz fluctuation in the isotopic mixing ratio, μmol mol^{-1}.
$c^{12\prime}$	20-Hz fluctuation in the $C^{16}O_2$ mixing ratio, μmol mol^{-1}.
CO_2	total carbon dioxide mole mixing ratio including all isotopologues, μmol mol^{-1}.
$C^{16}O_2$	carbon dioxide isotopologue (mass 44) mole mixing ratio, μmol mol^{-1}.
$^{13}CO_2$	carbon dioxide isotopologue (mass 45) mole mixing ratio, μmol mol^{-1}.
$C^{18}O^{16}O$	carbon dioxide isotopologue (mass 46) mole mixing ratio, μmol mol^{-1}.
$C_{wc}(f)$	cospectral density of vertical wind velocity and total CO_2 mole mixing ratio as a function of cyclic frequency (f), m s^{-1} μmol mol^{-1}.
$C_{wc^x}(f)$	cospectral density of vertical wind velocity and isotopic CO_2 mole mixing ratio as a function of cyclic frequency (f), m s^{-1} μmol mol^{-1}.
δ^x	isotopic composition of a sample in delta notation, ‰.
δ_a^x	isotopic composition of canopy air in delta notation, ‰.
δ_A^x	isotopic composition of net ecosystem photosynthetic flux in delta notation, (‰).
δ_N^x	isotopic composition of net ecosystem CO_2 exchange in delta notation, (‰).
δ_R^x	isotopic composition of ecosystem nonfoliar respiratory flux in delta notation, (‰).
$\overline{\delta_a^x}$	half-hourly block average of the isotopic composition of canopy air in delta notation, ‰.
$\delta_a^{x\prime}$	fluctuation (20 Hz) in the isotopic composition of canopy air in delta notation, ‰.
Δ^x	canopy-weighted photosynthetic discrimination, ‰.
λE	latent heat flux, W m^{-2}.
EC-IRGA	eddy covariance and infrared gas analyzer system (open path).
EC-TDL	eddy covariance and tunable diode laser system (closed path).

f cyclic frequency, Hz.
F_δ^x *isoflux*, net ecosystem isotopic CO_2 exchange, μmol m^{-2} s^{-1} ‰.
F_{GEP} gross ecosystem photosynthetic flux, μmol m^{-2} s^{-1}.
F_A net ecosystem photosynthetic flux, μmol m^{-2} s^{-1}.
F_N net ecosystem CO_2 exchange, μmol m^{-2} s^{-1}.
F_R nonfoliar ecosystem respiratory flux, μmol m^{-2} s^{-1}.
F_{TER} total ecosystem respiratory flux, μmol m^{-2} s^{-1}.
F_N^x net ecosystem isotopic CO_2 exchange, μmol m^{-2} s^{-1}.
F_{GEP}^x gross ecosystem isotopic CO_2 photosynthetic flux, μmol m^{-2} s^{-1}.
F_R^x nonfoliar isotopic CO_2 respiratory flux, μmol m^{-2} s^{-1}.
F_{TER}^x total ecosystem isotopic CO_2 respiratory flux, μmol m^{-2} s^{-1}.
G12 $C^{16}O_2$ gain factor, dimensionless.
G13 $^{13}CO_2$ gain factor, dimensionless.
G18 $C^{18}O^{16}O$ gain factor, dimensionless.
EC eddy covariance.
HTP high tank pressure (TDL reference gas).
IRGA infrared gas analyzer.
LTP low tank pressure (TDL reference gas).
ρ_a mean molar air density, mol m^{-3}.
Q_* net radiation, W m^{-2}.
REA relaxed eddy accumulation.
RMSE root mean squared error.
RSSE square root of the sum of squared residuals.
R^x absolute molar ratio of heavy to light isotope of a sample.
R_N^x absolute molar ratio of heavy to light isotope of net ecosystem CO_2 exchange.
R_A^x absolute molar ratio of heavy to light isotope of net photosynthetic CO_2 flux.
R_R^x absolute molar ratio of heavy to light isotope of nonfoliar CO_2 respiratory flux.
R_{VPDB} standard molar ratio, $^{13}C/^{12}C$ or $^{18}O/^{16}O$ based on the Vienna Peedee Belemnite scale.
S_c rate of change in total CO_2 storage between the ground and the EC measurement height, μmol m^{-2} s^{-1}.
S_c^x rate of change in isotopic CO_2 storage between the ground and the EC measurement height, μmol m^{-2} s^{-1}.
T_a air temperature, °C
TDL tunable diode laser.
u horizontal wind velocity, m s^{-1}.
u_* friction velocity, m s^{-1}.
σ_w standard deviation of the vertical wind velocity, m s^{-1}.
w vertical wind velocity, m s^{-1}.
$\overline{w'c'}$ mean covariance of vertical wind velocity and total CO_2 mole mixing ratio, m s^{-1} μmol mol^{-1}.
$\overline{w'c^{x'}}$ mean covariance of vertical wind velocity and isotopologue mole mixing ratio, m s^{-1} μmol mol^{-1}.

[63] **Acknowledgments.** We express our sincere thanks to Bill Breiter (USDA-ARS Biological Field Technician) for his assistance in the field and laboratory and Jim Brozowski, Travis Bavin, Jennifer Corcoran, Jeremy Smith, Kyounghee Kim, and Lisa Welp for their help deploying and maintaining the EC-TDL system and other ancillary equipment. We thank T. A. Black (University of British Columbia) for reviewing an early draft of this manuscript. We especially acknowledge the criticisms and helpful suggestions provided by D. R. Bowling (University of Utah) and two anonymous Reviewers. Financial support for this project was provided by the National Science Foundation, ATM-0546476 (T.J.G.), DEB-0514908 (X.L. and TJG), DEB-0514904 (X.L.) EAR-0229343 (X.L.), and the Office of Science (B.E.R.), U.S. Department of Energy, grant DE-FG02–03ER63684 (T.J.G. and J.M.B.).

References

Baker, J. M. (2000), Conditional sampling revisited, *Agric. For. Meteorol.*, *104*(1), 59–65, doi:10.1016/S0168-1923(00)00147-7.

Baker, J. M., and T. J. Griffis (2005), Examining strategies to improve the carbon balance of corn/soybean agriculture using eddy covariance and mass balance techniques, *Agric. For. Meteorol.*, *128*(3-4), 163–177, doi:10.1016/j.agrformet.2004.11.005.

Baldocchi, D. D., and D. R. Bowling (2003), Modelling the discrimination of $^{13}CO_2$ above and within a temperate broad-leaved forest canopy on hourly to seasonal time scales, *Plant Cell Environ.*, *26*, 231–244, doi:10.1046/j.1365-3040.2003.00953.x.

Blanken, P. D., T. A. Black, H. H. Neumann, G. den Hartog, P. C. Yang, Z. Nesic, R. Staebler, W. Chen, and M. D. Novak (1998), Turbulent flux measurements above and below the overstory of a boreal aspen forest, *Boundary Layer Meteorol.*, *89*, 109–140, doi:10.1023/A:1001557022310.

Bowling, D. R., D. D. Baldocchi, and R. K. Monson (1999), Dynamics of isotopic exchange of carbon dioxide in a Tennessee deciduous forest, *Global Biogeochem. Cycles*, *13*(4), 903–922, doi:10.1029/1999GB900072.

Bowling, D. R., P. P. Tans, and R. K. Monson (2001), Partitioning net ecosystem carbon exchange with isotopic fluxes of CO_2, *Global Change Biol.*, *7*(2), 127–145, doi:10.1046/j.1365-2486.2001.00400.x.

Bowling, D. R., S. D. Sargent, B. D. Tanner, and J. R. Ehleringer (2003), Tunable diode laser absorption spectroscopy for stable isotope studies of ecosystem-atmosphere CO_2 exchange, *Agric. For. Meteorol.*, *118*(1–2), 1–19, doi:10.1016/S0168-1923(03)00074-1.

Bowling, D. R., S. P. Burns, T. J. Conway, R. K. Monson, and J. W. C. White (2005), Extensive observations of CO_2 carbon isotope content in and above a high-elevation subalpine forest, *Global Biogeochem. Cycles*, *19*, GB3023, doi:10.1029/2004GB002394.

Farquhar, G. D., J. R. Ehleringer, and K. T. Hubick (1989), Carbon isotope discrimination and photosynthesis, *Annu. Rev. Physiol. Plant Mol. Biol.*, *40*, 503–537, doi:10.1146/annurev.pp.40.060189.002443.

Fung, I., et al. (1997), Carbon 13 exchanges between the atmosphere and biosphere, *Global Biogeochem. Cycles*, *11*(4), 507–533, doi:10.1029/97GB01751.

Gillon, J., and D. Yakir (2001), Influence of carbonic anhydrase activity in terrestrial vegetation on the ^{18}O content of atmospheric CO_2, *Science*, *291*(5513), 2584–2587, doi:10.1126/science.1056374.

Griffis, T. J., J. M. Baker, S. D. Sargent, B. D. Tanner, and J. Zhang (2004), Measuring field-scale isotopic CO_2 fluxes with tunable diode laser absorption spectroscopy and micrometeorological techniques, *Agric. For. Meteorol.*, *124*(1-2), 15–29, doi:10.1016/j.agrformet.2004.01.009.

Griffis, T. J., J. M. Baker, and J. Zhang (2005a), Seasonal dynamics of isotopic CO_2 exchange in C3/C4 managed ecosystem, *Agric. For. Meteorol.*, *132*(1-2), 1–19, doi:10.1016/j.agrformet.2005.06.005.

Griffis, T. J., X. Lee, J. M. Baker, S. Sargent, and J. Y. King (2005b), Feasibility of quantifying ecosystem-atmosphere $C^{18}O^{16}O$ exchange using laser spectroscopy and the flux-gradient method, *Agric. For. Meteorol.*, *135*(1-4), 44–60, doi:10.1016/j.agrformet.2005.10.002.

Griffis, T. J., J. Zhang, J. M. Baker, N. Kljun, and K. Billmark (2007), Determining carbon isotope signatures from micrometeorological measurements: Implications for studying biosphere-atmosphere exchange processes, *Boundary Layer Meteorol.*, *123*, 295–316, doi:10.1007/s10546-006-9143-8.

Hesterburg, R., and U. Siegenthaler (1991), Production and stable isotopic composition of CO_2 in soil near Bern Switzerland, *Tellus, Ser. B*, *43*, 197–205.

Hoefs, J. (2004), *Stable Isotope Geochemistry*, 244 pp., Springer, Berlin.

Kaimal, J. C., and J. J. Finnigan (1994), *Atmospheric Boundary Layer Flows: Their Structure and Measurement*, Oxford Univ. Press, New York.

Kaimal, J. C., J. C. Wyngaard, Y. Izumi, and O. R. Cote (1972), Spectral characteristics of surface layer turbulence, *Q. J. R. Meteorol. Soc.*, *98*, 563–589, doi:10.1002/qj.49709841707.

Katul, G. G., P. L. Finkelstein, J. F. Clarke, and T. G. Ellestad (1996), An investigation of the conditional sampling method used to estimate fluxes of active, reactive, and passive scalars, *J. Appl. Meteorol.*, *35*(10), 1835–1845, doi:10.1175/1520-0450(1996)035<1835:AIOTCS>2.0.CO;2.

Keeling, C. D. (1958), The concentration and isotopic abundances of atmospheric carbon dioxide in rural areas, *Geochim. Cosmochim. Acta*, *13*, 322–334, doi:10.1016/0016-7037(58)90033-4.

Knohl, A., R. A. Werner, W. A. Brand, and N. Buchmann (2005), Short-term variations in $\delta^{13}C$ of ecosystem respiration reveals link between assimilation and respiration in a deciduous forest, *Oecologia*, *142*, 70–82, doi:10.1007/s00442-004-1702-4.

Lee, X., T. A. Black, and M. D. Novak (1994), Comparison of flux measurements with open- and closed-path gas analyzers above an agricultural field and a forest floor, *Boundary Layer Meteorol.*, *67*, 195–202, doi:10.1007/BF00705514.

Lee, X., S. Sargent, R. Smith, and B. Tanner (2005), In-situ measurement of the water vapor $^{18}O/^{16}O$ isotope ratio for atmospheric and ecological applications, *J. Atmos. Oceanic Technol.*, *22*, 555–565, doi:10.1175/JTECH1719.1.

Lee, X., K. Kim, and R. Smith (2007), Temporal variations of the $^{18}O/^{16}O$ signal of the whole-canopy transpiration in a temperate forest, *Global Biogeochem. Cycles*, *21*, GB3013, doi:10.1029/2006GB002871.

Lenschow, D. H., and M. R. Raupach (1991), The attenuation of fluctuations in scalar concentrations through sampling tubes, *J. Geophys. Res.*, *96*(D8), 15,259–15,268, doi:10.1029/91JD01437.

Leuning, R., and M. J. Judd (1996), The relative merits of open- and closed-path analysers for measurement of eddy fluxes, *Global Change Biol.*, *2*(3), 241–253, doi:10.1111/j.1365-2486.1996.tb00076.x.

Leuning, R., and J. Moncrieff (1990), Eddy-covariance CO_2 flux measurements using open-path and closed-path CO_2 analyzers: Corrections for analyzer water-vapor sensitivity and damping of fluctuations in air sampling tubes, *Boundary Layer Meteorol.*, *53*, 63–76, doi:10.1007/BF00122463.

Liu, H. P., J. T. Randerson, J. Lindfors, W. J. Massman, and T. Foken (2006), Consequences of incomplete surface energy balance closure for CO_2 fluxes from open-path CO_2/H_2O infrared gas analyzers, *Boundary Layer Meteorol.*, *120*, 65–85, doi:10.1007/s10546-005-9047-z.

Lloyd, J., et al. (1996), Vegetation effects on the isotopic composition of the atmospheric CO_2 at local and regional scales: Theoretical aspects and a comparison between rain forest in Amazonia and a boreal forest in Siberia, *Aust. J. Plant Physiol.*, *23*, 371–399.

Mahrt, L. (1998), Flux sampling errors for aircraft and towers, *J. Atmos. Oceanic Technol.*, *15*(2), 416–429, doi:10.1175/1520-0426(1998)015<0416:FSEFAA>2.0.CO;2.

Massman, W. J. (1991), The attenuation of concentration fluctuations in turbulent-flow through a tube, *J. Geophys. Res.*, *96*(D8), 15,269–15,273, doi:10.1029/91JD01514.

Massman, W. J. (2000), A simple method for estimating frequency response corrections for eddy covariance systems, *Agric. For. Meteorol.*, *104*(3), 185–198, doi:10.1016/S0168-1923(00)00164-7.

Miller, J. B., and P. P. Tans (2003), Calculating isotopic fractionation from atmospheric measurements at various scales, *Tellus, Ser. B*, *55*, 207–214.

Murphey, B. F., and A. O. Nier (1941), Variations in the relative abundance of the carbon isotopes, *Phys. Rev.*, *59*(9), 771–772, doi:10.1103/PhysRev.59.771.2.

Nier, A. O. (1947), A mass spectrometer for isotope and gas analysis, *Rev. Sci. Instrum.*, *18*(6), 398–411, doi:10.1063/1.1740961.

Ogée, J., P. Peylin, M. Cuntz, T. Bariac, Y. Brunet, P. Berbigier, P. Richard, and P. Ciais (2004), Partitioning net ecosystem carbon exchange into net assimilation and respiration with canopy-scale isotopic measurements: An error propagation analysis with $^{13}CO_2$ and $CO^{18}O$ data, *Global Biogeochem. Cycles*, *18*, GB2019, doi:10.1029/2003GB002166.

Ponton, S., L. B. Flanagan, K. P. Alstad, B. G. Johnson, K. Morgenstern, N. Kljun, T. A. Black, and A. G. Barr (2006), Comparison of ecosystem water-use efficiency among Douglas-fir forest, aspen forest and grassland using eddy covariance and carbon isotope techniques, *Global Change Biol.*, *12*(2), 294–310, doi:10.1111/j.1365-2486.2005.01103.x.

Raupach, M. R. (1989), Stand overstorey processes, *Philos. Trans. R. Soc., Ser. B*, *324*(1223), 175–190, doi:10.1098/rstb.1989.0043.

Saleska, S. R., J. H. Shorter, S. Herndon, R. Jimenez, B. McManus, J. W. Munger, D. D. Nelson, and M. S. Zahniser (2006), What are the instrumentation requirements for measuring the isotopic composition of net ecosystem exchange of CO_2 using eddy covariance methods?, *Isotopes Environ. Health Stud.*, *42*(2), 115–133, doi:10.1080/10256010600672959.

Simpson, I. J., G. W. Thurtell, H. H. Neumann, G. den Hartog, and G. C. Edwards (1998), The validity of similarity theory in the roughness sublayer above forests, *Boundary Layer Meteorol.*, *87*(1), 69–99, doi:10.1023/A:1000809902980.

Swinbank, W. C. (1951), Measurement of vertical transfer of heat and water vapor by eddies in the lower atmosphere, *J. Meteorol.*, *8*, 135–145.

Tans, P. P., J. A. Berry, and R. F. Keeling (1993), Oceanic $^{13}C/^{12}C$ observation: A new window on ocean CO_2 uptake, *Global Biogeochem. Cycles*, *7*(2), 353–368, doi:10.1029/93GB00053.

Webb, E. K., G. I. Pearman, and R. Leuning (1980), Corrections of flux measurements for density effects due to heat and water vapour transfer, *Q. J. R. Meteorol. Soc.*, *106*, 85–100.

Welp, L. R., J. T. Randerson, and H. P. Liu (2006), Seasonal exchange of CO_2 and $\delta^{18}O$-CO_2 varies with postfire succession in boreal forest ecosystems, *J. Geophys. Res.*, *111*, G03007, doi:10.1029/2005JG000126.

Welp, L. R., X. Lee, K. Kim, T. J. Griffis, K. Billmark, and J. M. Baker (2008), $\delta^{18}O$ of evapotranspiration and the sites of leaf evaporation in a soybean canopy, *Plant Cell Environ.*, in press.

Werle, P., R. Mucke, and F. Slemr (1993), The limits of signal averaging in atmospheric trace-gas monitoring by tunable diode-laser absorption-spectroscopy (TDLAS), *Appl. Phys. B*, *57*(2), 131–139, doi:10.1007/BF00425997.

Yakir, D. (2003), The stable isotopic composition of atmospheric CO_2, in *Treatise on Geochemistry*, vol. 4, *The Atmosphere*, edited by R. F. Keeling, pp. 175–205, Elsevier, Oxford, U. K.

Yakir, D., and L. D. L. Sternberg (2000), The use of stable isotopes to study ecosystem gas exchange, *Oecologia*, *123*, 297–311, doi:10.1007/s004420051016.

Yakir, D., and X. F. Wang (1996), Fluxes of CO_2 and water between terrestrial vegetation and the atmosphere estimated from isotope measurements, *Nature*, *380*, 515–517, doi:10.1038/380515a0.

Zhang, J., T. J. Griffis, and J. M. Baker (2006), Using continuous stable isotope measurements to partition net ecosystem CO_2 exchange, *Plant Cell Environ.*, *29*, 483–496, doi:10.1111/j.1365-3040.2005.01425.x.

Zobitz, J. M., S. P. Burns, J. Ogée, M. Reichstein, and D. R. Bowling (2007), Partitioning net ecosystem exchange of CO_2: A comparison of a Bayesian/isotope approach to environmental regression methods, *J. Geophys. Res.*, *112*, G03013, doi:10.1029/2006JG000282.

J. M. Baker, K. Billmark, and T. J. Griffis, Department of Soil, Water, and Climate, University of Minnesota-Twin Cities, Borlaug Hall, 1991 Upper Buford Circle, St. Paul, MN 55108, USA. (tgriffis@umn.edu)

J. Greene, S. D. Sargent, E. Swiatek, and B. D. Tanner, Campbell Scientific, Inc., 815 West 1800 North, Logan, UT 84321, USA.

X. Lee, School of Forestry and Environmental Studies,Yale University, 21 Sachem Street, New Haven, CT 06520, USA.